RESEARCH ARTICLE

Identification of the MuRF1 Skeletal Muscle Ubiquitylome Through Quantitative Proteomics

Leslie M. Baehr [1,†], David C. Hughes [1,†], Sarah A. Lynch[2],
Delphi Van Haver [3,4,5], Teresa Mendes Maia[3,4,5], Andrea G. Marshall[1],
Lilliana Radoshevich [6], Francis Impens[3,4,5], David S. Waddell [2], Sue
C. Bodine [1,*]

[1]Department of Internal Medicine, Division of Endocrinology and Metabolism, Carver College of Medicine, University of Iowa, Iowa City, IA 52242, USA, [2]Department of Biology, University of North Florida, 1 UNF Drive, Jacksonville, FL 32224, USA, [3]Department of Biomolecular Medicine, Ghent University, Ghent, Belgium, [4]VIB Center for Medical Biotechnology, Ghent, Belgium, [5]VIB Proteomics Core, Ghent, Belgium and [6]Department of Microbiology and Immunology, Carver College of Medicine, University of Iowa, Iowa City, IA 52242, USA

*Address correspondence to S.C.B. (e-mail: sue-bodine@uiowa.edu)
†These authors contributed equally to this work.

Abstract

MuRF1 (TRIM63) is a muscle-specific E3 ubiquitin ligase and component of the ubiquitin proteasome system. MuRF1 is transcriptionally upregulated under conditions that cause muscle loss, in both rodents and humans, and is a recognized marker of muscle atrophy. In this study, we used in vivo electroporation to determine whether MuRF1 overexpression alone can cause muscle atrophy and, in combination with ubiquitin proteomics, identify the endogenous MuRF1 substrates in skeletal muscle. Overexpression of MuRF1 in adult mice increases ubiquitination of myofibrillar and sarcoplasmic proteins, increases expression of genes associated with neuromuscular junction instability, and causes muscle atrophy. A total of 169 ubiquitination sites on 56 proteins were found to be regulated by MuRF1. MuRF1-mediated ubiquitination targeted both thick and thin filament contractile proteins, as well as, glycolytic enzymes, deubiquitinases, p62, and VCP. These data reveal a potential role for MuRF1 in not only the breakdown of the sarcomere but also the regulation of metabolism and other proteolytic pathways in skeletal muscle.
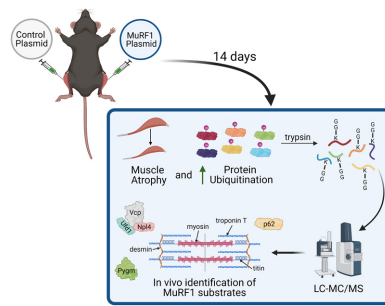
Key words: muscle atrophy; MuRF1; electroporation; ubiquitin proteomics; protein degradation

Introduction

The ubiquitin proteasome system (UPS) plays an important role in all cells, but is particularly critical in skeletal muscle for regulating homeostasis and remodeling. The UPS is made up of E1, E2, and E3 enzymes that coordinate the conjugation of ubiquitin to a substrate protein. Ubiquitin is covalently attached to lysine residues that can be a proteolytic or nonproteolytic signal depending on the number and linkage of the ubiquitin molecules.[1] The addition of 4 or more ubiquitin molecules linked via lysine 48, resulting in a polyubiquitin chain, typically targets a protein for degradation by the 26S proteasome. The specificity of ubiquitination is determined by the E3 ligase, which brings together an E2 enzyme and a substrate protein through protein–protein interaction domains or adaptor proteins that recruit the substrate protein.[2] UPS activity has been shown to be essential for the maintenance of skeletal muscle fiber integrity and function.[3] Furthermore, regulation of muscle fiber size is dependent on the UPS, as increases in activity occur in response to both growth and atrophy stimuli.[4–6]

MuRF1 (TRIM63) is a muscle-specific E3 ubiquitin ligase that was first identified as a novel Really Interesting New Gene (RING) finger protein capable of binding to the giant myofibrillar protein titin near its kinase domain.[7] MuRF1 has 2 closely related family members, MuRF2 (TRIM55) and MuRF3 (TRIM54), that all belong to the tripartite motif (TRIM) family of proteins. The protein structure of the MuRF family is characterized by a tripartite fold of the RING, B-box, and coiled-coil (CC) domains, followed by a C-terminal acidic tail.[8] The RING domain allows for interaction with E2 enzymes and promotes ubiquitin transfer.[2] The B-box domain is important for dimerization and the Cos-box flanking the CC domain may be important for localization of MuRF1 within the sarcomere.[8,9] MuRF1 has been shown to localize to the Z-disk and M-line of the sarcomere, and to colocalize with endocytic acetylcholine receptors near the neuromuscular junction.[7,8,10] MuRF1 can also translocate to the nucleus, a process that may require SUMOylation.[11]

In skeletal muscle, MuRF1 has been shown to be a robust marker of muscle atrophy. MuRF1, along with MAFbx/Atrogin-1 (Fbxo32), was one of the first two E3 ligases found to be upregulated under a number of atrophy-inducing conditions and *MuRF1*$^{-/-}$ mice spare muscle mass following denervation and glucocorticoid treatment.[12–15] MuRF1 is also an important regulator of cardiac size, as *MuRF1*$^{-/-}$ mice display physiological hypertrophy of the heart, which may be due to a decrease in proteasome activity.[16] Based on these findings, it has long been presumed that upregulation of *MuRF1* leads to muscle atrophy by increasing polyubiquitinated proteins and targeting them for degradation by the proteasome. In response to denervation

and fasting, MuRF1 has been suggested to promote disassembly of the sarcomere by ubiquitinating the myosin stabilizing proteins myosin-binding protein C (MyBP-C), myosin essential light chain 1 (MyLC1), and myosin regulatory light chain 2 (MyLC2).[17] A number of other myofilament and metabolic proteins have been identified as MuRF1 substrates using in vitro methods such as yeast two-hybrid (Y2H) screens, but it is unclear whether these proteins are also substrates in vivo. The complete set of substrates targeted for ubiquitination by MuRF1 remains poorly defined, and thus the mechanisms by which upregulation of MuRF1 contributes to muscle atrophy are still poorly understood.

Identification of the substrates targeted by a specific E3 ligase is challenging; however, new technologies have been developed, such as Gly-Gly (diGly) remnant affinity purification, coupled with liquid chromatography followed by tandem mass spectrometry (LC-MS/MS) to identify sites of modification on target proteins.[18] Digestion of ubiquitinated proteins by trypsin leaves a diglycine remnant on the side chain of ubiquitinated lysine residues (K-ε-GG). The development of monoclonal antibodies specific to the K-ε-GG epitope has made it possible to enrich for ubiquitinated peptides after trypsinization. One limitation of this method, however, is that the K-ε-GG epitope is also generated following trypsin digestion of ISG15 and NEDD8-modified proteins.[18,19] In this study, we combined *MuRF1* overexpression with enrichment of endogenous ubiquitin sites using LC-MS/MS to assist in the identification of the full list of MuRF1 substrates in skeletal muscle. We show that overexpression (OE) of *MuRF1* in tibialis anterior (TA) muscle results in muscle atrophy and that mutations in the RING domain abolish this atrophy promoting phenotype. Further, we discovered 169 lysine sites on 56 proteins that were regulated by *MuRF1* OE. The list of putative substrates includes contractile proteins associated with both the thick and thin myofilament, as well as, proteins associated with metabolism and proteolysis. The discovery that MuRF1 ubiquitinates the autophagy-associated protein p62/SQSTM1 and the endoplasmic reticulum–associated degradation protein VCP/p97 suggests that MuRF1 may coordinate the regulation of additional proteolytic pathways in skeletal muscle.

Methods

Animal Protocols

Male C57BL/6 mice were obtained from Charles River laboratories at ages 12–16 weeks and used for in vivo electroporation experiments within 2 weeks of their arrival. Validation studies were performed in male *MuRF1*$^{-/-}$ mice obtained from a breeding colony maintained at the University of Iowa. *MuRF1*$^{-/-}$

mice at 15 months of age were used for electroporation experiments and at 5 months of age for the denervation experiment. $MuRF1^{-/-}$ mice are on a C57BL/6 background and their generation has been previously described.[12] Animals were housed in ventilated cages (Thoren Caging Systems) at 21°C with 12 h light/12 h dark cycles and had ad libitum access to standard chow (Harlan Teklad formula 7013) and water throughout the study. All animal procedures were approved by the Institutional Animal Care and Use Committee of the University of Iowa.

In Vivo Electroporation

Transfection of mouse skeletal muscle with plasmid DNA was performed as previously described.[20–22] Briefly, after a 2 h pretreatment with 0.4 units/μL of bovine placental hyaluronidase (Sigma) resuspended in sterile 0.9% saline, 20 μg of plasmid DNA was injected into the TA muscle; the hind limbs were placed between 2-paddle electrodes and subjected to 10 pulses (20 ms) of 175 V/cm using an ECM-830 electroporator (BTX Harvard Apparatus). For electroporation experiments involving untagged plasmids, 2 μg of emGFP was also injected to identify transfected fibers. Following transfection, mice were returned to their cages to resume normal activities until tissue collection at 7, 14, and 30 days posttransfection.

Denervation

Targeted denervation of the lower limb muscles in the right leg was accomplished through transection of the sciatic nerve as previously described.[23] Under isoflurane anesthesia (2%–4% inhalation) and with the use of aseptic surgical techniques, the sciatic nerve was isolated in the midthigh region and cut with sharp scissors. Mice were given an analgesic (buprenorphine, 0.1 mg/kg) immediately following the surgery and returned to their cage following recovery.

Tissue Collection

Following completion of the appropriate time period, mice were anesthetized with isoflurane, and muscles were excised, weighed, frozen in liquid nitrogen, and stored at −80°C for biochemical analysis. TA muscles excised for histology were processed as described below. On completion of tissue removal, mice were euthanized by exsanguination.

Immunohistochemistry and Tissue Analysis

TA muscles harvested for histological evaluation were immediately fixed in 4% (w/v) paraformaldehyde for 16 h at 4°C. Following a sucrose gradient incubation period, the TA muscles were embedded in tissue freezing medium (Triangle Biomedical Sciences) and 10 μm serial sections were taken from the muscle midbelly using a cryostat (Thermo HM525). For laminin staining, TA muscle sections were permeabilized in phosphate buffer solution with 1% triton (PBST) for 10 min at room temperature. After washing with PBST, sections were blocked with 5% goat serum for 15 min at room temperature. Sections were incubated with anti-Laminin (1:500, Sigma, L9393) in 5% goat serum for 2 h at room temperature, followed by two 5-min washes with PBS. Goat anti-rabbit AlexaFluor® 555 secondary (1:333) in 5% goat serum was then added for 1 h at room temperature. Slides were cover slipped using ProLong Gold Antifade reagent (Invitrogen). All sections were examined and photographed using a Nikon Eclipse Ti automated inverted microscope equipped

with NIS-Elements BR digital imaging software. Image analysis was performed using MyoVision software.[24] Skeletal muscle fiber size was analyzed by measuring ≥350 transfected muscle fibers per muscle, per animal (10× magnification). Transfected muscle fibers were identified as green fluorescent protein (GFP)-positive as shown in Figures 1 and 2. Nontransfected (GFP-negative) fibers were considered for cross-sectional area (CSA) analysis; however, many of the muscles displayed a very high transfection efficiency with few GFP-negative fibers within the same region as GFP-positive fibers for comparison. Thus, fiber size comparisons were made between GFP-positive fibers in the empty vector (EV) and MuRF1 OE transfected muscles.

Confocal imaging (Zeiss LSM710) of TA sections was performed using a 40× oil-immersion lens, for a total magnification of 400×. Signal in the 488 channel was optimized using a single $MuRF1$ OE section as a reference. Once set, settings remained the same across all images captured.

Plasmid Generation

The open reading frames of murine MuRF1 and MAFbx were amplified from cDNA generated using RNA isolated from C2C12 cells using the primers listed in Table S5. Total RNA was isolated from C2C12 myoblasts using the RNeasy Mini kit (Qiagen, Valencia, CA) according to the manufacturer's instructions. Purified total RNA was reverse transcribed to cDNA using M-MLV Reverse Transcriptase and a Poly T primer according to the manufacturer's protocol (Thermo Fisher Scientific). The MuRF1 cDNA was subsequently subcloned into the EcoRI and XbaI sites of pcDNA3.1(+) (Thermo Fisher Scientific). The MAFbx cDNA was subcloned into the EcoRI and XbaI sites of pcDNA3.1(+) (Thermo Fisher Scientific). The MuRF1 and MAFbx cDNAs were sequenced to confirm the absence of mutations and correct orientation (Thermo Fisher Scientific). MuRF1 was fused to GFP by cloning the cDNA of MuRF1 into the HindIII and BamHI sites of pEGFP-C3 and sequenced to confirm in-frame fusion between the MuRF1 and GFP open reading frames. A 6× myc tag was added to the N-terminus of MuRF1 by cloning the cDNA of MuRF1 into the XhoI and XbaI sites of the pCS2+MT plasmid and sequencing to confirm in-frame fusion between the myc tag sequences and the MuRF1 open reading frame.

Site-directed mutagenesis was used to create the C44S/C47S RING domain mutant of MuRF1 in the pcDNA3.1(+) and pEGFP-C3 expression plasmids using the primers listed in Table S5. The QuikChange II Site-Directed Mutagenesis protocol was performed using 200 ng of plasmid DNA and PfuTurbo DNA Polymerase according to the manufacturer's protocol (Agilent Technologies, Santa Clara, CA) followed by Dpn I (New England Biolabs) digest and transformation into competent cells (New England Biolabs). All constructs were sequenced to confirm successful mutation (Eurofins Genomics).

RNA Isolation and qPCR

To assess the effect of $MuRF1$ OE on gene transcription, RNA was isolated from frozen TA muscle powder using RNAzol RT reagent (Sigma-Aldrich, St Louis, MO) in accordance with the manufacturer's instructions. cDNA was synthesized using the iScript Reverse Transcription Supermix kit (Bio-Rad, Hercules, CA) from 1 μg of total RNA. PCR reactions (10 μL) were set up as: 2 μL of cDNA, 0.5 μL (10 μM stock) forward and reverse primer, 5 μL of Power SYBR Green master mix (Thermo Fisher Scientific), and 2 μL of RNA/DNA free water. Gene expression analysis was then performed by quantitative PCR on a QuantStudio
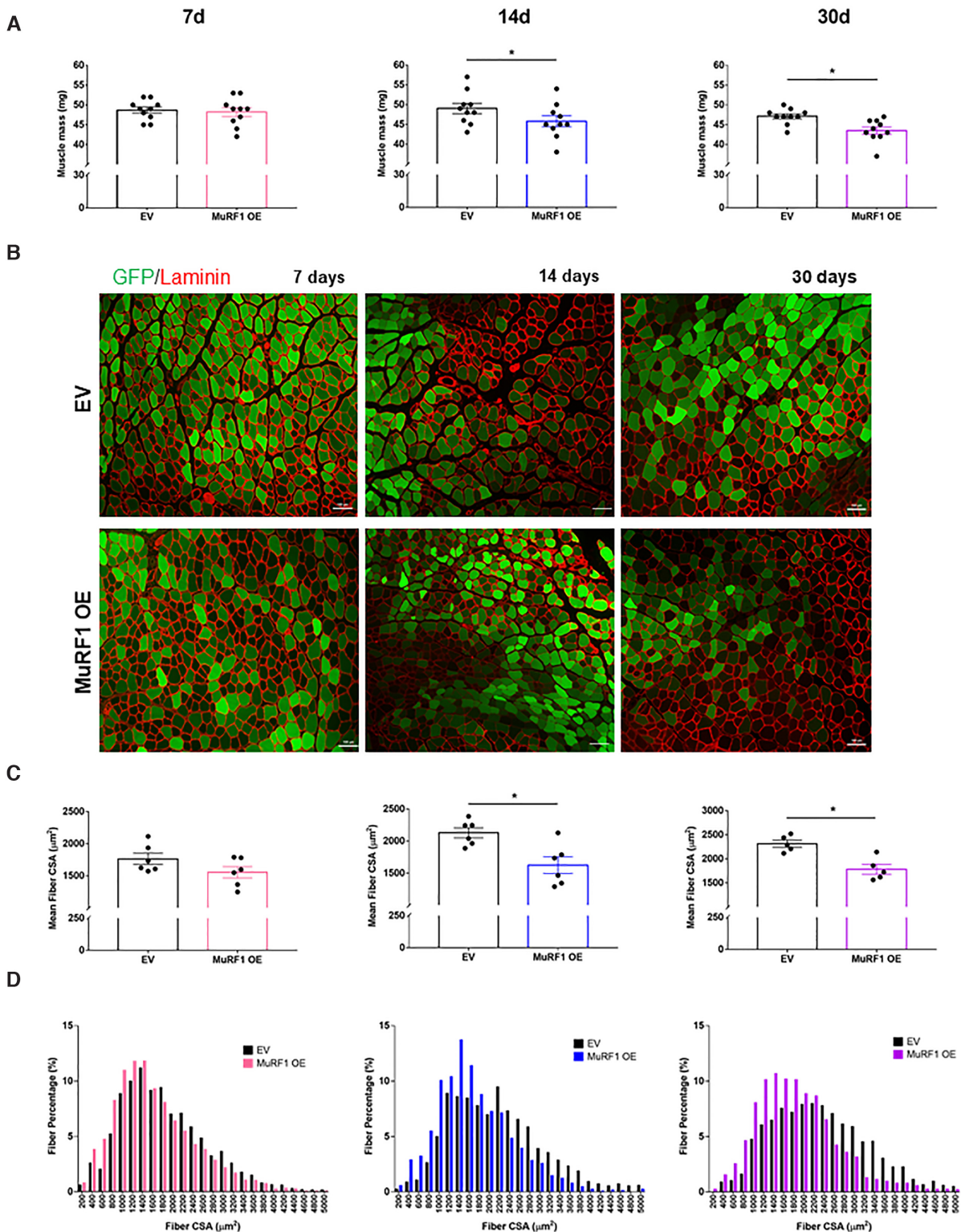
Figure 1. Overexpression of *MuRF1* Results in Muscle Atrophy. **(A)** Mass of mouse tibialis anterior (TA) muscles transfected with either an empty vector (EV) control plasmid or untagged MuRF1 plasmid for 7 (left), 14 (middle), and 30 (right) days; $n = 10$/time point. OE, overexpression. Data are presented as mean $\pm$ standard error of measure (SEM) with individual data points included. *P*-values were calculated using a one-tailed paired Student's *t*-test, *$P \leq .003$. **(B)** Representative images of TA cross sections electroporated with an EV or untagged MuRF1 plasmid for 7 (left), 14 (middle), and 30 (right) days and stained for laminin (red). An emGFP plasmid was included in the electroporation to identify transfected fibers. Scale bars, 100 μm; $n = 5$–6/time point. **(C)** Quantification of mean fiber cross-sectional area (CSA) of GFP-positive TA muscle fibers electroporated with an EV or untagged MuRF1 plasmid for 7 (left), 14 (middle), and 30 (right) days; $n = 6$ for 7- and 14-day time points, $n = 5$ for 30-day time point. Data are presented as mean $\pm$ SEM with individual data points included. *P*-values were calculated using a one-tailed paired Student's *t*-test, *$P \leq .0075$. **(D)** Distributions of fiber CSA of GFP-positive TA muscle fibers electroporated with an EV or untagged MuRF1 plasmid for 7 (left), 14 (middle), and 30 (right) days; $n = 6$ for 7- and 14-day time points, $n = 5$ for 30-day time point.
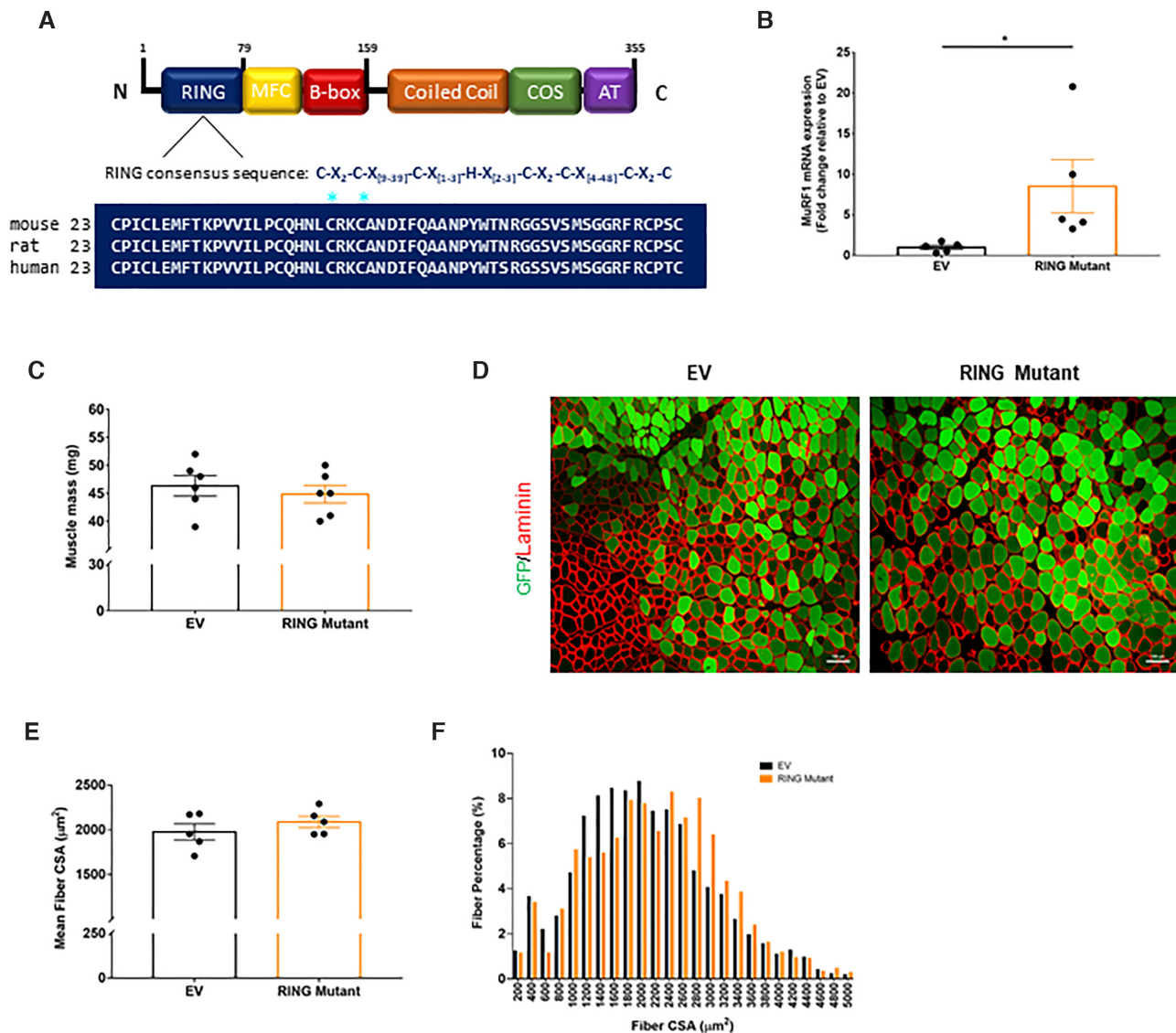
Figure 2. Mutation of the RING Domain of MuRF1 Prevents Muscle Atrophy. **(A)** Schematic of the domain structure of MuRF1. The consensus sequence of the RING domain is shown, along with the mouse, rat, and human MuRF1 RING domain sequences. "∗" indicates the cysteine residues that were mutated to create the RING mutant plasmid. MFC, MuRF family domain; COS, C-terminal subgroup One Signature; AT, C-terminal acidic tail. **(B)** Expression of *MuRF1* in mouse tibialis anterior (TA) muscles transfected with an empty vector (EV) control plasmid or untagged MuRF1 RING mutant plasmid for 14 days; $n = 5$/group. Data are presented as mean ± SEM with individual data points included. P-values were calculated using a one-tailed paired Student's t-test, *$P \le .0463$. **(C)** Mass of mouse TA muscles transfected with an EV plasmid or untagged MuRF1 RING mutant plasmid for 14 days; $n = 6$/group. Data are presented as mean ± SEM with individual data points included. **(D)** Representative images of TA cross sections electroporated with an EV or untagged MuRF1 RING mutant plasmid for 14 days and stained for laminin (red). An emGFP plasmid was included in the electroporation to identify transfected fibers. Scale bars, 100 μm; $n = 5$/group. **(E)** Quantification of mean fiber cross-sectional area (CSA) of GFP-positive TA muscle fibers electroporated with an EV or untagged MuRF1 RING mutant plasmid for 14 days; $n = 5$/group. Data are presented as mean ± SEM with individual data points included. **(F)** Distributions of fiber CSA of GFP-positive TA muscle fibers electroporated with an EV or untagged MuRF1 RING mutant plasmid; $n = 5$/group.

6 Flex Real-time PCR System (Applied Biosystems, Foster City, CA) using the mouse primers shown in Table S5. PCR cycling comprised: hold at 50°C for 5 min, 10 min hold at 95°C, before 40 PCR cycles of 95°C for 15 s followed by 59°C for 30 s and 72°C for 30 s. For MUSK and HDAC4, an annealing temperature of 60°C was used. Melt curve analysis at the end of the PCR cycling protocol yielded a single peak. As a result of reference gene instability, gene expression was normalized to tissue weight and subsequently reported as the fold change relative to control muscles, as described previously. This type of analysis has previously been used extensively by our group.[25–27]

Fractionation of Muscle Tissue

Separation of myofibrillar and sarcoplasmic protein fractions was performed according to the optimized protocol described by Roberts et al.[28] Briefly, 10 volumes of ice-cold buffer 1 (25 mM Tris, pH 7.2, 0.5% Triton X-100) were added to 10–15 mg of frozen TA muscle powder and homogenized using a Bullet Blender (Next Advance). The homogenate was then centrifuged at 1500 × *g* for 10 min at 4°C. Following centrifugation, the supernatant (sarcoplasmic fraction) was placed into a new tube and the pellet was resuspended in 10 volumes of ice-cold buffer 1 as a wash step. The resuspended pellet was centrifuged at 1500 ×

g for 10 min at 4°C and the supernatant was discarded. The pellet was then resuspended in 15 volumes of ice-cold buffer 2 (20 mM Tris–HCl, pH 7.2, 100 mM KCl, 20% glycerol, 1 mM DTT, 50 mM spermidine). After a quick 1 min spin on a desktop centrifuge, the supernatant (myofibrillar fraction) was transferred to a new tube.

Cytosolic and nuclear protein fractions were extracted from frozen TA muscle powder by first homogenizing in STM buffer (1 M sucrose, 1 M Tris, pH 7.4, 1 M $MgCl_2$, water, and protease inhibitors). The homogenate was centrifuged at 800 × *g* for 15 min. The supernatant was transferred to a new tube and centrifuged for 10 min at 11 000 × *g*. Following centrifugation, the supernatant was transferred to a new tube and labeled "cytosolic fraction." The pellet from the initial centrifugation was resuspended in STM buffer and vortexed for 15 s. The resuspended pellet was centrifuged at 800 × *g* for 15 min. The supernatant was then discarded and the pellet was resuspended in STM buffer, followed by 2 cycles of centrifugation as described above. Following the final centrifugation, the pellet was resuspended in NET Buffer (1 M HEPES, 1 M $MgCl_2$, 3 M NaCl, 100 mM EDTA, Glycerol, 1% Triton-X 100, water, and protease inhibitors). The resulting mixture was sonicated for 10 s and then centrifuged at 11 000 × *g* for 15 min. The supernatant was transferred to a new tube and labeled "nuclear fraction."

Protein concentrations of each fraction were measured using the Pierce 660 nm protein assay (Thermo Fisher Scientific) according to the manufacturer's instructions. Isolated fractions were separated by SDS-PAGE for immunoblotting (see below).

Immunoprecipitation

Frozen TA muscle powder was homogenized in lysis buffer (50 mM Tris, pH 7.6, 100 mM NaCl, 1 mM dithiothreitol, 0.5% Triton X-100) with added protease and phosphatase inhibitors (Thermo Fisher Scientific). Following homogenization, the samples were centrifuged at 12 000 × *g* for 20 min. The supernatant was collected and protein concentrations were measured using the Pierce 660 nm protein assay (Thermo Fisher Scientific) according to the manufacturer's instructions. Immunoprecipitation (IP) was carried out using the Dynabeads Protein G protocol (Invitrogen). Briefly, 5 μg of mouse FK2 (Enzo, BML-PW8810) or normal mouse IgG (Santa Cruz Biotechnology, sc-2025) was diluted in 200 μL PBS with 0.02% Tween-20 (PBST) and incubated with 50 μL Dynabeads Protein G with rotation for 20 min at room temperature. Following 1 wash with PBST, 800 μg of total protein was added to the beads and incubated with rotation for 20 min at room temperature. After washing 3 times with PBST, the beads were resuspended in 100 μL of PBST and moved to a clean microcentrifuge tube. The protein bound to the beads was then eluted and denatured using 20 μL of elution buffer and 10 μL of premixed NuPAGE LDS Sample Buffer and NuPAGE Sample Reducing Agent (Invitrogen). The samples were heated for 10 min at 70°C and then loaded onto a gel for immunoblotting.

Immunoblotting

For immunoblotting, 4–10 μg of sarcoplasmic and myofibrillar protein fractions, IP samples, or 16 μg of total TA protein denatured in 4× laemmli sample buffer (2% input) were subjected to SDS-PAGE using 4%–20% Mini-PROTEAN TGX or Criterion TGX stain-free gels (Bio-Rad). The protein was then transferred onto polyvinylidene difluoride membrane. Membranes were blocked in 3% nonfat milk in Tris-buffered saline with 0.1% Tween-20 added for 1 h, followed by incubation with primary

antibody overnight at 4°C. The membranes were then washed and incubated with anti-rabbit or anti-mouse HRP-conjugated secondary antibodies for 1 h at room temperature. Immobilon Western Chemiluminescent HRP substrate (Millipore) was added to the membranes and image acquisition was performed using the Azure C400 System (Azure Biosystems). Band quantification was performed using Image Lab 6.0.1 software (Bio-Rad). Total protein staining of the membrane was used as the normalization control for each blot. Images of the total protein stains can be found in Figures S4–S6. A list of the primary antibodies used in this study is provided in Table S6. The dilutions utilized for the primary antibodies were: α-actinin (1:1000), Desmin (1:500), Desmuslin (1:1000), Fen1 (1:1000), FK2 (1:1000), GAPDH (1:1000), Klhl31 (1:500), LDHA (1:1000), MyBPC2 (1:1000), Myc-tag (1:1000), Nploc4/Npl4 (1:1000), PSMA6 (1:1000), SQSTM1/p62 (1:1000), Telethonin (1:1000), Uchl1 (1:1000), Ufd1 (1:1000), Usp5 (1:1000), VCP (1:1000), MyHC (1:1000), MyLC2 (0.5 μg/μL), and Troponin T (0.5 μg/μL). Anti-rabbit IgG, HRP-linked (1:10 000, Cell Signaling, 7074) and anti-mouse IgG, HRP-linked (1:10 000, Cell Signaling, 7076) were used as secondary antibodies.

Proteomics Sample Preparation

Four C57BL/6 mice were electroporated with the untagged MuRF1 plasmid in 1 TA muscle and an empty vector (control) plasmid in the contralateral TA muscle. After 14 days, the mice were anesthetized with isoflurane, and the TA muscles were excised, weighed, and frozen in liquid nitrogen. All tissues collected from these experiments were exclusively used for proteomics. Whole muscles were homogenized in 5 mL urea lysis buffer containing 9 M urea and 20 mM HEPES, pH 8.0. The samples were sonicated with 3 pulses of 15 s at an amplitude of 20% using a 3 mm probe, with incubation on ice for 1 min between pulses. After centrifugation for 15 min at 20 000 × *g* at room temperature to remove insoluble components, proteins were reduced by addition of 5 mM DTT and incubation for 30 min at 55°C and then alkylated by addition of 10 mM chloroacetamide and incubation for 15 min at room temperature in the dark. The protein concentration was measured using a Bradford assay (Bio-Rad), and from each sample 13.8 mg protein was used to continue the protocol. Samples were further diluted with 20 mM HEPES pH 8.0 to a final urea concentration of 4 M, and proteins were digested with 69 μg LysC (Wako) (1/200, w/w) for 4 h at 37°C. Samples were again diluted to 2 M urea and digested with 69 μg trypsin (Promega) (1/200, w/w) overnight at 37°C. The resulting peptide mixture was acidified by addition of 1% trifluoroacetic acid (TFA) and after 15 min incubation on ice, samples were centrifuged for 15 min at 1780 × *g* at room temperature to remove insoluble components. Immuno-capture of Gly-Gly-modified peptides was then performed using the PTMScan® Ubiquitin Remnant Motif (K-ε-GG) Kit (Cell Signaling Technology) according to the manufacturer's instructions. Briefly, peptides were purified on Sep-Pak C18 cartridges (Waters), lyophilized for 2 days, and redissolved in 1.4 mL 1× IP buffer supplied with the kit. Note that at this point, aliquots corresponding to 200 μg of digested protein material were taken for shotgun proteomics analysis. Peptides were incubated with the antibody-bead slurry for 2 h on a rotator at 4°C and after several wash steps, diglycine modified peptides were eluted in 100 μL 0.15% TFA and desalted on reversed phase C18 OMIX tips (Agilent), all according to the manufacturer's protocol. Purified diglycine modified peptides were dried under vacuum in HPLC inserts, and stored at −20°C until LC-MS/MS analysis.

LC-MS/MS and Data Analysis

Purified peptides for shotgun analysis were redissolved in 20 μL solvent A (0.1% TFA in water/ACN (98:2, v/v) and peptide concentration was determined on a Lunatic spectrophotometer (Unchained Labs).[29] Two micrograms of each sample was injected for LC-MS/MS analysis on an UltiMate 3000 RSLCnano system in-line connected to an Orbitrap Fusion Lumos mass spectrometer (Thermo) equipped with a pneu-Nimbus dual ion source (Phoenix S&T). Trapping was performed at 10 μL/min for 4 min in solvent A on a 20 mm trapping column (made in-house, 100 μm internal diameter (I.D.), 5 μm beads, C18 Reprosil-HD, Dr. Maisch, Germany) and the sample was loaded on a 200 cm long micro pillar array column (PharmaFluidics) with C18-endcapped functionality mounted in the UltiMate 3000's column oven at 50°C. For proper ionization, a fused silica PicoTip emitter (10 μm inner diameter) (New Objective) was connected to the μPAC outlet union and a grounded connection was provided to this union. Peptides were eluted by a nonlinear increase from 1% to 55% MS solvent B (0.1% FA in water/ACN (2:8, v/v)) over 145 min, first at a flow rate of 750 nL/min, then at 300 nL/min, followed by a 10 min wash reaching 99% MS solvent B and reequilibration with MS solvent A (0.1% FA in water). The mass spectrometer was operated in data-dependent mode, automatically switching between MS and MS/MS acquisition. Full-scan MS spectra (300–1500 m/z) were acquired in TopSpeed with a 3 s acquisition cycle at a resolution of 120 000 in the Orbitrap analyzer after accumulation to a target AGC value of 200 000 with a maximum injection time of 30 ms. The precursor ions were filtered for charge states (2–7 required), dynamic range (60 s; +/− 10 ppm window), and intensity (minimal intensity of 3E4). The precursor ions were selected in the multipole with an isolation window of 1.2 Da and accumulated to an AGC target of 5E3 or a maximum injection time of 40 ms and activated using HCD fragmentation (34% NCE). The fragments were analyzed in the Ion Trap Analyzer at normal scan rate.

Purified diglycine modified peptides were redissolved in 20 μL solvent A of which 15 μL was injected for LC-MS/MS analysis on an UltiMate 3000 RSLCnano system in-line connected to a Q Exactive HF mass spectrometer (Thermo). Trapping was performed at 10 μL/min for 4 min in solvent A on a 20 mm trapping column (made in-house, 100 μm internal diameter (I.D.), 5 μm beads, C18 Reprosil-HD, Dr. Maisch, Germany) and the sample was loaded on a 200 cm long micro pillar array column (PharmaFluidics) with C18-endcapped functionality mounted in the UltiMate 3000's column oven at 50°C. For proper ionization, a fused silica PicoTip emitter (10 μm inner diameter) (New Objective) was connected to the μPAC outlet union and a grounded connection was provided to this union. Peptides were eluted by a nonlinear increase from 1% to 55% MS solvent B (0.1% FA in water/acetonitrile (2:8, v/v)) over 116 min, first at a flow rate of 750 nL/min, then at 300 nL/min, followed by a 14 min wash reaching 99% MS solvent B and reequilibration with MS solvent A (0.1% FA in water). The mass spectrometer was operated in data-dependent mode, automatically switching between MS and MS/MS acquisition for the 8 most abundant ion peaks per MS spectrum. Full-scan MS spectra (375–1500 m/z) were acquired at a resolution of 60 000 in the orbitrap analyzer after accumulation to a target value of 3 000 000. The 8 most intense ions above a threshold value of 8300 were isolated (window of 1.5 Th) for fragmentation at a normalized collision energy of 28% after filling the trap at a target value of 100 000 for maximum 120 ms. MS/MS spectra (200–2000 m/z) were acquired at a resolution of 15 000 in the orbitrap analyzer. The S-lens RF level was set at 50 and we excluded precursor ions with single, unassigned and >7 charge states from fragmentation selection. QCloud was used to control instrument longitudinal performance during the project.[30]

Data analysis was performed with MaxQuant (version 1.6.3.4)[31] using the Andromeda search engine with default search settings including a false discovery rate set at 1% on the peptide and protein level. Two different searches were performed to analyze the spectra from the diglycine-enriched samples and the shotgun samples. In both searches, spectra were interrogated against the mouse proteins in the Swiss-Prot Reference Proteome database (database release version of June 2019 containing 22 282 mouse protein sequences, (http://www.uniprot.org)). The mass tolerance for precursor and fragment ions was set to 4.5 and 20 ppm, respectively, during the main search. Enzyme specificity was set as C-terminal to arginine and lysine, also allowing cleavage at proline bonds with a maximum of 3 missed cleavages. Variable modifications were set to oxidation of methionine residues, acetylation of protein N-termini and GlyGly modification of lysine residues, while carbamidomethylation of cysteine residues was set as fixed modification. Matching between runs was enabled with a matching time window of 0.7 min and an alignment time window of 20 min. Only proteins with at least 1 unique or razor peptide were retained leading to the identification of 1412 proteins and 13 329 GlyGly modified sites. Proteins were quantified by the MaxLFQ algorithm integrated in the MaxQuant software. A minimum ratio count of 2 unique or razor peptides was required for quantification.

Further data analysis of the shotgun results was performed with the Perseus software (version 1.6.2.1) after loading the protein groups file from MaxQuant. Reverse database hits were removed, LFQ intensities were log2 transformed, and replicate samples were grouped. Proteins with less than 3 valid values in at least 1 group were removed, and missing values were imputed from a normal distribution around the detection limit leading to a list of 844 quantified proteins that was used for further data analysis (Table S1). Then, SAM testing was used (FDR = 0.05 and s0 = 1 cutoff values were considered for test significance)[32] to compare control and MuRF1 samples and a volcano plot was generated. Twenty-four proteins were found to be significantly regulated. For the analysis of the diglycine modified peptide data, the GlyGly(K)Sites file was loaded in the Perseus software (version 1.6.2.1). Reverse hits were removed, the site table was expanded, the intensity values were log2 transformed, and the median was subtracted. Replicate samples were grouped, GlyGly(K)sites with less than 3 valid values in at least 1 group were removed, and missing values were imputed from a normal distribution around the detection limit leading to a list of 963 quantified GlyGly peptides that was used for further data analysis. Then, SAM tests were performed (FDR = 0.05 and s0 = 1 cutoffs) to compare control and MuRF1 samples and a volcano plot was generated. One hundred sixty-nine GlyGly peptides were significantly regulated and plotted in a heat map after nonsupervised hierarchical clustering. Gene ontology (GO) term enrichment analyses were performed using DAVID (database for annotation, visualization, and integrated discovery)[33,34] on both the list of proteins with upregulated ubiquitylation peptides and with downregulated peptides, using an EASE score cutoff of 0.1. Proteins from all quantified ubiquitylated peptides served as background list for the analyses.

Statistics

Results are presented as mean ± standard error of measure (SEM), with individual values included on each graph. Statistical differences for all in vivo overexpression studies were determined using a one- or two-tailed paired Student's *t*-test. A one-way ANOVA with Tukey's post hoc test was used to determine statistical differences in protein levels across the time course of MuRF1 overexpression. Analyses were performed using Graph-Pad Prism v.7.00 software. $*P \leq .05$ was used to define statistical significance. The IP experiments shown in Figure 5A and B were not subjected to statistics due to the small sample size. The statistics used for the analysis of the proteomics data are discussed in the proteomics method section.

Results

MuRF1 Overexpression Causes Muscle Atrophy After 14 Days

MuRF1 is transcriptionally upregulated during skeletal muscle atrophy, but it remains unclear whether *MuRF1* OE alone can cause muscle atrophy. To determine whether MuRF1 alone can trigger muscle atrophy, we electroporated an untagged MuRF1 expression plasmid into the TA muscle of male C57BL/6 mice and assessed the effect after 7, 14, and 30 days. An EV plasmid was electroporated into the contralateral TA muscle as a control. Expression of *MuRF1* was significantly increased at all 3 time points, with the greatest increase observed 14 days after electroporation (Figure S1A–C). After 7 days, no significant decreases in TA muscle mass or fiber size were detected (Figure 1A–D, left panels); however, a trend toward smaller fiber CSA was observed (−9%). After 14 days of *MuRF1* OE, we detected significant decreases in muscle mass (−6.6%) and CSA (−23%) of transfected fibers compared with fibers in the contralateral TA that were transfected with an EV plasmid (Figure 1A–D, middle panels). Muscle atrophy was still present after 30 days, with the loss of muscle mass (−9%) and fiber CSA (−22%) similar to that observed at day 14 (Figure 1A–D, right panels). To eliminate the possibility that endogenous *MuRF1* was activated by the transfection of the MuRF1 plasmid and contributed to the observed atrophy, we electroporated the untagged MuRF1 plasmid into the TA of male *MuRF1*$^{-/-}$ mice. After 14 days, OE of *MuRF1* caused significant loss of TA muscle mass and mean fiber CSA in *MuRF1*$^{-/-}$ mice (Figure S2).

MAFbx/Atrogin-1 is another muscle-specific E3 ubiquitin ligase that shows an expression pattern similar to MuRF1 during muscle atrophy.[12] Therefore, we sought to determine whether *MAFbx* OE also leads to muscle atrophy. Transfection of an untagged MAFbx expression plasmid into the TA muscle for 14 days did not result in a change in muscle mass or fiber CSA, despite a >20-fold increase in *MAFbx* expression (Figure S3).

Mutation of the RING Finger Domain in the MuRF1 Gene

E3 ubiquitin ligases generally fall into one of two classes based on the presence of a HECT or RING domain.[35] The canonical sequence of the RING domain is shown in Figure 2A and is located near the N-terminus of MuRF1. The RING domain of MuRF1 is highly conserved between mouse, rat, and human and is critical for binding with E2 conjugating enzymes and catalyzing the transfer of ubiquitin from the E2 to substrate proteins.[2] Without a functional RING domain, MuRF1 would theoretically

cease to function as an E3, resulting in less ubiquitination and attenuated degradation of muscle proteins during atrophy. This is supported by the observation that both *MuRF1*$^{-/-}$ mice and mice expressing a MuRF1 RING domain deletion mutant protein exhibited less muscle atrophy upon denervation.[12,17] To expand these findings, we created a MuRF1 RING mutant plasmid to determine whether mutations of 2 conserved cysteine residues within the RING domain sequence are sufficient to disrupt MuRF1 function (Figure 2A). These 2 cysteines are found in the α-helix portion of the RING domain and are important for coordination of the first zinc ion required for ubiquitin transfer.[2] In addition, the α-helix is a part of the E2-binding interface.[2] Unlike with the MuRF1 untagged plasmid, electroporation of an untagged RING mutant expression plasmid in basal skeletal muscle did not cause muscle atrophy. Despite a significant increase in *MuRF1* expression, no decreases in muscle mass or fiber size were observed after 14 days (Figure 2B–F). Similar findings were observed when the untagged RING mutant plasmid was transfected into the TA muscle of *MuRF1*$^{-/-}$ mice (Figure S2). These results indicate that a functional RING domain is required to induce muscle atrophy.

Muscle Protein Ubiquitination and Increases in Transcription of Atrophy-Associated Genes with MuRF1 Overexpression

Due to an inability to find a specific MuRF1 antibody, we confirmed the expected increase in MuRF1 and RING mutant protein after 14 days of electroporation using myc-tagged MuRF1 and myc-tagged RING mutant plasmids. A similar reduction in TA muscle mass was observed after transfection of myc-MuRF1 for 14 days, indicating that addition of the epitope tag did not alter MuRF1 function (Figure S1D). Analogous to the untagged RING mutant plasmid, OE of the myc-tagged RING mutant plasmid for 14 days did not cause muscle atrophy (Figure S1E). Interestingly, multiple higher molecular weight bands were visible for MuRF1 and the RING mutant, with the majority of bands ranging from ∼60 to 150 kDa (predicted molecular weight of 6×-myc MuRF1 is 46 kDa) (Figure 3A). Also visible were a number of bands below 37 kDa, especially for the RING mutant protein, which are most likely protein degradation products. Separation of the cytoplasmic and nuclear fractions using the myc-tagged plasmids revealed MuRF1, at various sizes, to be present in both fractions and mutation of the RING domain did not prevent translocation of MuRF1 into the nucleus (Figure 3B). Visualization of MuRF1 and the RING mutant using GFP-tagged plasmids revealed distinct distribution patterns in TA muscle cross sections. After 14 days, MuRF1 is highly concentrated around the edge of the fibers in a "U" shaped pattern, but can also be found in other regions of the fiber such as the myofilaments. In contrast, the RING mutant is more diffuse and can be seen throughout the fibers (Figure 3C). In particular, the RING mutant appears to remain attached to the myofilaments. GFP-tagged plasmids induced similar changes to muscle mass as the untagged plasmids (Figure S1F and G).

Despite the lack of significant muscle atrophy, OE of *MuRF1* for 7 days resulted in significant increases in the ubiquitination of sarcoplasmic and myofibrillar proteins, and this increased ubiquitination was maintained through 30 days of *MuRF1* OE (Figure 3D). After OE of the RING mutant for 14 days, an increase in ubiquitinated proteins was also found in the sarcoplasmic fraction, but not in the myofibrillar fraction (Figure 3D).

Given that MuRF1 has been reported to play a role in acetylcholine receptor (AChR) turnover and can be upregulated by
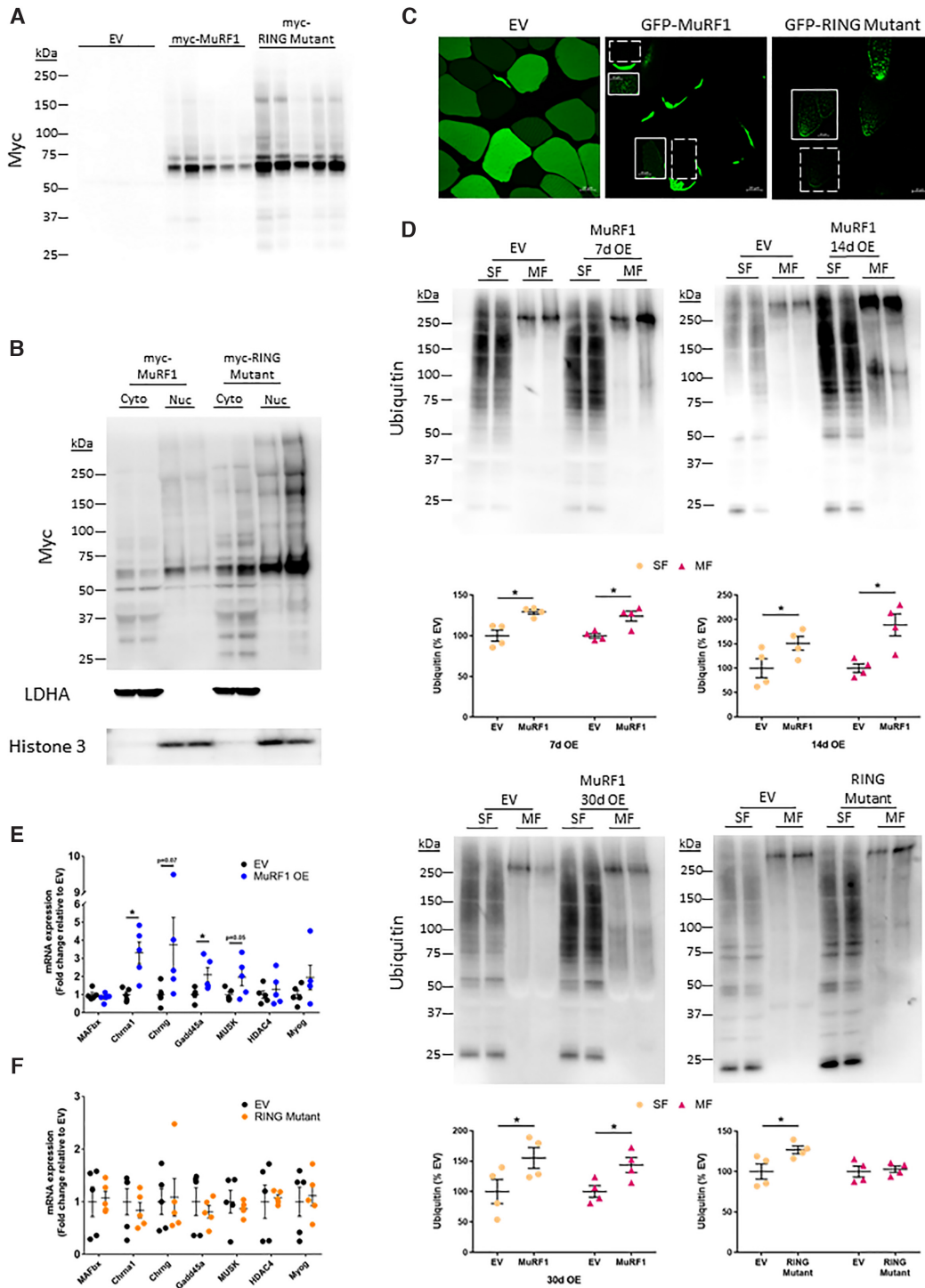
Figure 3. *MuRF1* Overexpression Increases Muscle Protein Ubiquitination and Neuromuscular Junction Instability. **(A)** Western blot of MuRF1 and MuRF1 RING mutant proteins after electroporation of an empty vector (EV) control plasmid, myc-MuRF1 plasmid, or myc-MuRF1 RING mutant plasmid into the tibialis anterior (TA) muscle for 14 days; $n = 5$/group. **(B)** Representative Western blot of cytoplasmic and nuclear localization of MuRF1 and MuRF1 RING mutant proteins following electroporation of their respective myc-tagged plasmids into the TA for 14 days; $n = 4$/group. LDHA and Histone 3 were used to confirm complete separation of the 2 fractions. **(C)** Representative confocal images of TA cross sections electroporated with EV, GFP-MuRF1, or GFP-MuRF1 RING mutant plasmids for 14 days. An emGFP plasmid was included in the electroporation of the EV to identify transfected fibers. Dashed boxes indicate location of magnified regions shown in adjacent white bordered boxes. Scale bars, 20 μm; $n = 5$/group. **(D)** Representative Western blots and quantification of ubiquitinated proteins from the sarcoplasmic and myofibrillar fractions of TA muscles electroporated with an EV or untagged MuRF1 plasmid for 7, 14, and 30 days, or an EV or untagged MuRF1 RING mutant plasmid for 14 days; $n = 4$/group. Data are presented as mean ± SEM with individual data points included. P-values were calculated using a one-tailed unpaired Student's t-test, $^*P \leq .0395$. OE, overexpression. qPCR analysis of *MAFbx* and genes associated with neuromuscular junction instability in TA muscles electroporated for 14 days with an **(E)** EV or untagged MuRF1 plasmid or **(F)** an EV or untagged MuRF1 RING mutant plasmid; $n = 5$/group. Data are presented as mean ± SEM with individual data points included. P-values were calculated using a two-tailed paired Student's t-test, $^*P \leq .0361$. P-values are included where $.05 < P < .1$.

myogenin during denervation,[10,36,37] we assessed expression of a number of genes related to neuromuscular junction instability. After 14 days, *Chrna1* and *Gadd45a* were found to be significantly upregulated by *MuRF1* OE (Figure 3E). *Chrng* and *MUSK* gene expression was also increased but did not reach significance. No change in expression was found for any of the genes analyzed following OE of the RING mutant (Figure 3F) or after OE of MuRF1 for 7 and 30 days (Figure S1H and I). The activation of Gadd45a at 14 days is noteworthy given its association with muscle atrophy.[38,39]

Identification of MuRF1 Substrates Through Diglycine Ubiquitin Adduct Enrichment and LC-MS/MS

The endogenous substrates of MuRF1 in skeletal muscle have not yet been systemically mapped. To date, the majority of substrates linked to MuRF1 have been identified through Y2H screens and immunoprecipitations using a tagged MuRF1 protein.[17,40–42] These substrates include MyBP-C, MyLC1, MyLC2, and myosin heavy chain (MyHC), along with metabolic enzymes such as muscle creatine kinase (M-CK), pyruvate dehydrogenase (PDH), and glycogen phosphorylase (PYGM). Interestingly, some MuRF1 substrates may be tissue specific, as troponin I has been shown to be degraded by MuRF1 in cardiac muscle, but not in skeletal muscle.[43] More recently, MuRF1 substrates in cardiomyocytes were identified through the use of tandem ubiquitin-binding entities (TUBEs) technology, which allows for the isolation of polyubiquitinated proteins.[44] While a number of novel substrates were identified, one limitation with this technique is that it does not recognize mono or diubiquitinated proteins and MuRF1 has been shown to monoubiquitinate PPARα in the heart.[45] Thus, in an attempt to identify the full set of in vivo MuRF1 targets and their modification sites, we coupled electroporation of full-length MuRF1 with diglycine enrichment of ubiquitinated peptides and identification by label-free quantitative mass spectrometry. TA muscles transfected with the untagged MuRF1 plasmid or the EV (control) for 14 days underwent trypsin digestion, and peptides carrying diglycine ubiquitin remnant motifs were isolated by immunoenrichment. The diglycine modified peptides were then identified and quantified by label-free LC-MS/MS. A total of 963 ubiquitination sites, corresponding to 250 proteins, were quantified from the TA muscle (Table S2). For 143 proteins, we detected only a single ubiquitination site, while on the remaining proteins we found multiple sites, including titin that was modified at more than 150 positions (Figure 4A). Statistical analysis revealed that OE of *MuRF1* resulted in significant upregulation of 153 ubiquitination sites on 45 proteins and significant downregulation of 16 sites on 11 proteins (Figure 4B and Tables 1 and 2) compared with EV control. Nonsupervised hierarchical clustering of these significantly regulated sites indicate that the majority are completely absent in the control muscles (shown in gray in Figure 4C), strongly suggesting that they are MuRF1-specific ubiquitination sites. While we were able to confirm a number of proteins that were previously reported as MuRF1 substrates, most of our identified ubiquitination sites are found on proteins that have not been previously linked to MuRF1 (Tables 1 and 2). Furthermore, we found that almost half of the significantly regulated ubiquitination sites were located on titin. Another protein found to have multiple ubiquitination sites was MuRF1 itself. This was not surprising given its autocatalytic capabilities,[7,9,44] but it was interesting to note that of the 23 lysines located within the MuRF1 protein sequence, 16 were found to be ubiquitinated.

When mapped to the different domains of MuRF1, all domains, except for the acidic tail, were shown to contain at least 1 ubiquitination site, with the majority of sites being located within the coiled-coil domain (Figure 4D). The coiled-coil domain is required for MuRF1 dimerization and for its binding to the A168–170 region of titin.[7,46,47] GO analysis of the putative MuRF1 substrates (ie, the 45 proteins with significantly upregulated ubiquitin sites) revealed a significant enrichment for muscle contraction and ubiquitin-dependent catabolism as GO terms under biological process, and the VCP-Ufd1–Npl4 complex was highlighted in the GO analysis for cellular compartments (Figure 4E). VCP is part of the AAA (ATPases associated with diverse cellular activities) family and has been shown to extract ubiquitinated proteins from membranes and other cellular structures, such as chromatin, which often results in their degradation by the proteasome.[48,49] VCP is also involved in ER-associated degradation and has been implicated in the degradation of muscle proteins during atrophy.[48,50] VCP interacts with a number of cofactors, 2 of which are Ufd1 and Npl4. Ufd1 and Npl4 contain ubiquitin-binding domains and act to recruit substrates to VCP.[48] All 3 members of the VCP–Ufd1–Npl4 complex are ubiquitinated by MuRF1 (Table 1).

Validation of MuRF1 Substrates

Based on our list of substrates, MuRF1 targets a diverse array of proteins within muscle fibers. Interestingly, a large number of these substrates play some role within the UPS. In addition to VCP, ubiquitination of several deubiquitinases, including ubiquitin carboxyl-terminal hydrolase 5 (Usp5) and 13 (Usp13), along with ubiquitin carboxyl-terminal hydrolase isozyme L1 (Uchl1), was increased in response to *MuRF1* OE. Similarly, the kelch-like proteins 31 and 41, which act as substrate adaptors for the Cullin RING E3 ubiquitin ligases, and proteasome subunit alpha type 6, which is a subunit of the 20S proteasome, were found to have lysine residues with increased ubiquitination in response to *MuRF1* OE. Furthermore, OE of *MuRF1* led to increased ubiquitination on 2 sites of p62, the autophagy-related protein that is capable of binding to ubiquitinated proteins and shuttling them to the proteasome or autophagosome for degradation.[51] p62 has previously been shown to be a substrate of MuRF1 and to work with MuRF1 to regulate the turnover of AChRs.[10,52,53] Previously, VCP was found to interact with MuRF1 in a Y2H screen, but the authors were unable to confirm a direct interaction between the 2 proteins.[53] To validate a subset of substrates identified through our proteomics analysis, we determined whether OE of *MuRF1* increased the ubiquitination of p62, VCP, and kelch-like protein 31 (Klhl31), which to our knowledge has not been linked to MuRF1. We examined the ubiquitination of these target proteins in the TA muscle after 7 and 14 days of *MuRF1* OE. For all 3 substrates, OE of *MuRF1* resulted in increased ubiquitination at both time points (Figure 5A). Interestingly, the ubiquitination of Klhl31 further increased between 7 and 14 days, but it is unclear whether MuRF1 is solely responsible for this observed increase in Klhl31 ubiquitination. It is possible that the initial ubiquitination by MuRF1 led to further ubiquitination by another E3 ligase.

In contrast to *MuRF1* OE, we were interested in knowing whether the absence of *MuRF1* altered the ubiquitination of its substrates under atrophy conditions. Since VCP and p62 have been shown to increase with denervation[50,54] and both can bind to and transport ubiquitinated proteins to the proteasome, we examined whether ubiquitination of these 2 proteins differed between wild-type (WT) and *MuRF1*^{−/−} mice after 7 days of denervation. Ubiquitination of p62 was similar between WT and
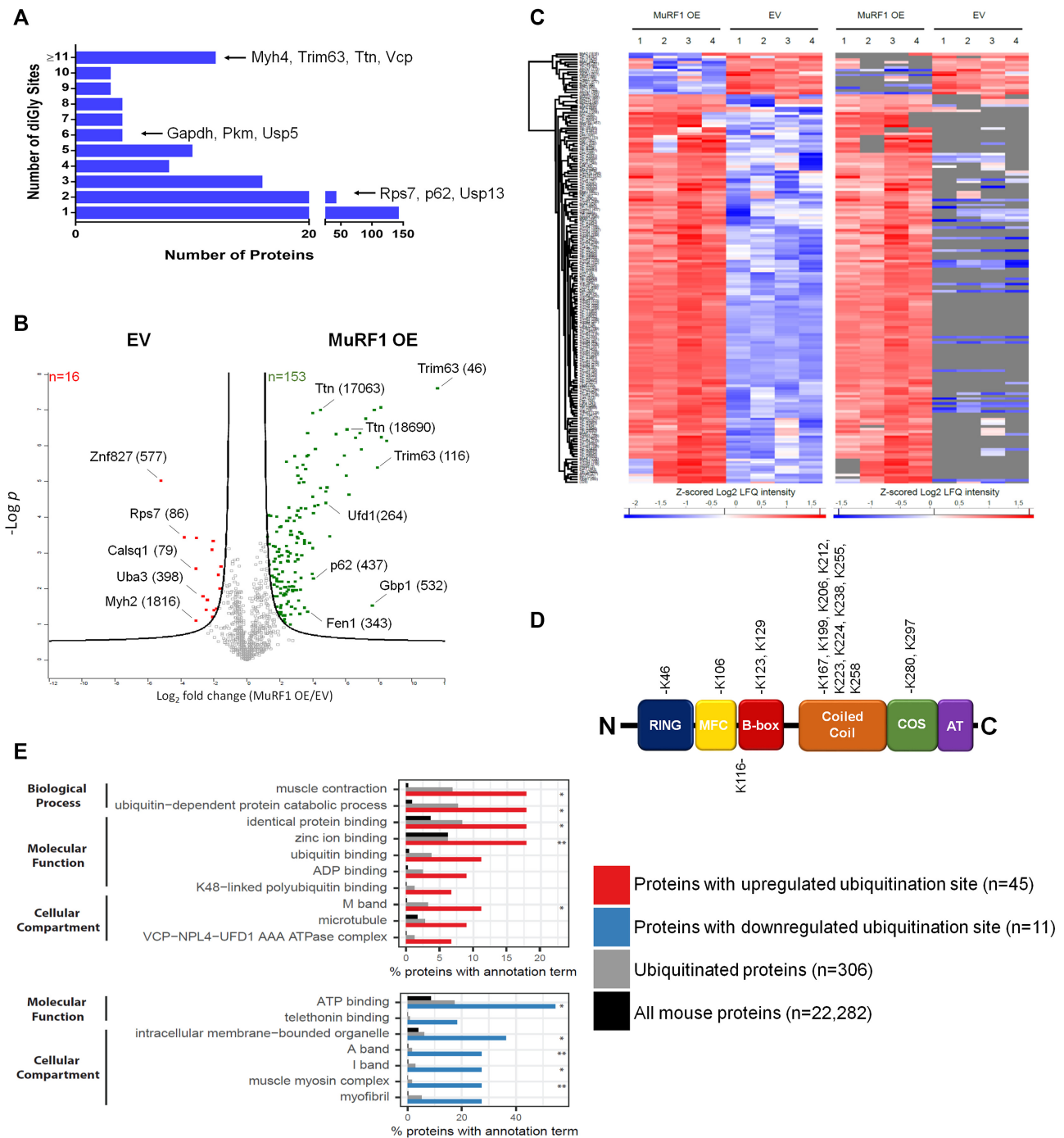
Figure 4. Identification of In Vivo MuRF1 Ubiquitination Sites on Substrate Proteins. **(A)** Comparison of the number of diglycine sites per protein identified from the tibialis anterior (TA) muscles electroporated with an empty vector (EV) control plasmid or untagged MuRF1 plasmid for 14 days; $n = 4$/group. A total of 963 diglycine sites on 250 proteins were identified and quantified by LC-MS/MS. **(B)** Volcano plot showing the 153 significantly upregulated diglycine sites and the 16 significantly downregulated diglycine sites. The log2 fold change of each diglycine site is shown on the x-axis and the log P-value is shown on the y-axis. Some of the upregulated and downregulated sites are labeled with their gene name and the lysine position of the identified diglycine site is included in parentheses. **(C)** Heat map visualization of the 169 significantly regulated diglycine sites after nonsupervised hierarchical clustering. On the right, the same heat map is shown with missing values in gray. **(D)** Schematic of the domain structure of MuRF1 (taken from Figure 2A) with the location of the lysine residues containing significantly upregulated diglycine sites. **(E)** Gene ontology analysis of the upregulated (red) and downregulated (blue) ubiquitinated proteins relative to all proteins with quantified ubiquitinated peptides identified in this study (gray) and all mouse proteins in the Swiss-Prot Reference Proteome database. The analysis was done with DAVID (database for annotation, visualization, and integrated discovery). Each bar corresponds to the percentage of proteins annotated with each GO term. An EASE score of 0.1 was used to highlight GO terms and those terms that reached significance have been identified: *EASE score <0.05; **EASE score <0.01.

Table 1. Identification of Proteins and the Corresponding Lysine Residue(s) that had Increased Ubiquitination Following Overexpression of MuRF1 for 14 Days

Protein ID	Protein Name	Gene Name	Lysine Position within Protein
Q38HM4	MuRF1[a]	*Trim63*	46, 106, 116, 123, 129, 167, 199, 206, 212, 223, 224, 238, 255, 258, 280, 297
G3X8Y1	MuRF2	*Trim55*	8, 293
Q9ERP3	MuRF3	*Trim54*	8, 49, 168, 210, 262, 289, 295
A2ASS6	Titin[a]	*Ttn*	2492, 7434, 8224, 9198, 13446, 15756, 16650, 17063, 17448, 17519, 18085, 18590, 18690, 19472, 20174, 20495, 20532, 20542, 20543, 21256, 21435, 21458, 21631, 21921, 21944, 21952, 22093, 23046, 24128, 24505, 24530, 24925, 24942, 25263, 25272, 25464, 25587, 25773, 26292, 26599, 26689, 26814, 26832, 26850, 27043, 27236, 27460, 27654, 27751, 28155, 28268, 28688, 28834, 29292, 30099, 30247, 30428, 30935, 31051, 32104, 32242, 32463, 32635
Q5SX40	Myosin 1	*Myh1*	1232
G3UW82	Myosin 2[a]	*Myh2*	506, 848
Q5SX39	Myosin 4	*Myh4*	924, 1229, 1358
Q62234	Myomesin-1	*Myom1*	415
Q14BI5	Myomesin-2	*Myom2*	966
P31001	Desmin	*Des*	43, 108, 286, 298, 308, 338
P21107	Tropomyosin alpha-3 chain	*Tpm3*	66
Q9QZ47	Troponin T, fast skeletal muscle	*Tnnt3*	75
P97457	Myosin regulatory light chain 2, skeletal muscle isoform[a]	*Mylpf*	105, 112
Q9JMH9	Unconventional myosin-XVIIIa	*Myo18a*	457
P18760	Cofilin-1	*Cfl1*	92
Q01853	Translational endoplasmic reticulum ATPase	*Vcp*	18, 231, 389, 668
P70362	Ubiquitin fusion degradation protein 1	*Ufd1*	264
P60670	Nuclear protein localization protein 4	*Nploc4*	545
Q5BKP2	Ubiquitin carboxyl-terminal hydrolase 13	*USP13*	638
P56399	Ubiquitin carboxyl-terminal hydrolase 5[a]	*USP5*	20
Q9R0P9	Ubiquitin carboxyl-terminal hydrolase isozyme L1	*Uchl1*	4
P62983	Ubiquitin 40S ribosomal protein S27a	*Rps27a*	48, 63
Q9QUM9	Proteasome subunit alpha type 6	*Psma6*	102
Q61510	E3 ubiquitin/ISG15 ligase TRIM25	*Trim25*	284, 289, 291, 300
Q64337	Sequestosome-1/p62[a]	*Sqstm1*	13, 437
Q923T9	Calcium/calmodulin-dependent protein kinase II subunit gamma	*Camk2g*	246
P14824	Annexin A6	*Anxa6*	377
P39749	Flap endonuclease 1	*Fen1*	343
Q8BWA5	Kelch-like protein 31	*Klhl31*	12
A2AUC9	Kelch-like protein 41	*Klhl41*	583
P16858	Glyceraldehyde 3 phosphate dehydrogenase	*Gapdh*	143
Q9WUB3	Glycogen phosphorylase, muscle form[a]	*Pygm*	248
P06151	L-lactate dehydrogenase A chain	*Ldha*	243, 245
P52480	Pyruvate kinase	*Pkm*	166
P63017	Heat shock cognate 71 kDa protein	*Hspa8*	3
P62259	14-3-3 protein epsilon	*Ywhae*	106
O08539	Myc box-dependent-interacting protein 1	*Bin1*	272
Q3UH93	Plexin-D1	*Plxnd1*	1657
Q811D0	Disks large homolog 1	*Dlg1*	392
O35309	N-myc-interactor	*Nmi*	230
A0A140LIF8	Immunity-related GTPase family M member 2	*Irgm2*	328
Q2EMV9	Protein mono-ADP-ribosyltransferase	*Parp14*	1532
Q91WQ3	Tyrosine-tRNA ligase	*Yars*	513
Q01514	Interferon-induced guanylate-binding protein 1	*Gbp1*	532
Q9D8C4	Interferon-induced 35 kDa protein homolog	*Ifi35*	57

[a]Previously identified as a MuRF1 substrate using in vitro methods.

Table 2. Identification of Proteins and the Corresponding Lysine Residue(s) that had Decreased Ubiquitination Following Overexpression of MuRF1 for 14 Days

Protein ID	Protein Name	Gene Name	Lysine Position within Protein
A2ASS6	Titin	*Ttn*	14197, 17122, 17426, 18740
G3UW82	Myosin 2	*Myh2*	1816
Q5SX40	Myosin 1	*Myh1*	642
Q9JK37	Myozenin-1	*Myoz1*	233
Q8R429	Sarcoplasmic/endoplasmic reticulum calcium ATPase 1	*Atp2a1*	365, 511, 713
O09165	Calsequestrin-1	*Casq1*	79
Q9CZW4	Long-chain fatty acid–CoA ligase 3	*Acsl3*	96
P14142	Solute carrier family 2, facilitated glucose transporter member 4	*Slc2a4*	261
P62082	40S ribosomal protein S7	*Rps7*	86
Q8C878	NEDD8-activating enzyme E1 catalytic subunit	*Uba3*	398
Q505G8	Zinc finger protein 827	*Znf827*	577

MuRF1$^{-/-}$ mice following denervation; however, ubiquitination of VCP was decreased in the *MuRF1*$^{-/-}$ mice (Figure 5B). In addition, we noted that VCP protein levels were not increased in the *MuRF1*$^{-/-}$ denervated muscles.

The Majority of MuRF1 Substrates Are Not Degraded Following Ubiquitination

Shotgun analysis of our tryptic peptides prior to diglycine enrichment indicated that *MuRF1* OE did not result in a decrease in substrate protein levels. Excluding MuRF1, only 24 proteins were found to be increased or decreased after 14 days of *MuRF1* OE and only 1 of these proteins (Uchl1) was also identified as a MuRF1 substrate (Tables S3 and S4). Notably, *MuRF1* OE resulted in an increase in Uchl1 protein. To expand on the proteomics data, we examined the protein content of a number of MuRF1 substrates in a separate set of TA muscles after 7, 14, and 30 days of *MuRF1* OE. Interestingly, the protein levels for many of the substrates normally localized in the sarcoplasm were found to increase at 14 or 30 days (Figure 5C and D), and only 1 sarcomere-bound substrate, MyLC2, was found to decrease after 14 days of *MuRF1* OE (Figure 5E and F). However, we did find a significant increase in contractile protein levels in the sarcoplasmic (soluble) fraction with *MuRF1* OE. Moreover, some of these proteins were identified as substrates of MuRF1 (desmin, troponin T), while others were not (desmuslin, telethonin), although telethonin has been previously shown by others to be a substrate of MuRF1[42,55] (Figure 5E and F). An increase in these soluble contractile proteins likely indicates that they have been released from the sarcomere and will ultimately be degraded.[56] Loss of these contractile proteins would explain how *MuRF1* OE causes muscle atrophy. OE of the RING mutant did not result in an increase in these contractile proteins within the soluble fraction. This can be explained by our previous finding that ubiquitination of the myofibrillar fraction did not increase with RING mutant OE (Figure 3D). The RING mutant is likely unable to generate a degradation signal and thus, muscle atrophy does not occur due to the sarcomere being left intact. Collectively, our proteomics data have identified a number of novel MuRF1 substrates, and subsequent analyses suggest that ubiquitination by MuRF1 alone may not be adequate to direct certain substrates for degradation.

Discussion

Muscle atrophy is the result of a complex and tightly regulated process in which muscle fibers become smaller as sarcomeres are disassembled and contractile proteins are degraded. The muscle-specific E3 ligase, MuRF1, is quickly upregulated in response to atrophy signals and is thought to be critical in initiating the breakdown of muscle by ubiquitinating and targeting thick filament proteins for degradation.[12,17] Here, we further highlight the importance of MuRF1 in muscle atrophy by showing that overexpression of *MuRF1* alone leads to an increase in ubiquitinated proteins and a significant loss in fiber CSA. The only other study to examine the effect of *MuRF1* OE on muscle mass was by Hirner et al., who generated a transgenic mouse line on the FVBN background strain that overexpressed human MuRF1 selectively in skeletal muscle (MuRF1-Tg).[40] They found no difference in whole body mass or mass of the quadriceps muscle of WT and MuRF1-Tg at 8 weeks of age. However, at 20 weeks of age, MuRF1-Tg mice were 7% ($P < .005$) lighter in body weight than WT mice. Unfortunately, no further analysis of muscle mass or fiber CSA was performed in the 20-week-old mice.

In the present study, we utilized ubiquitin proteomics to identify the set of proteins modified by *MuRF1* overexpression in vivo, ie, the MuRF1 ubiquitylome. Our results indicate that after 14 days of *MuRF1* OE, 153 ubiquitination sites on 45 different proteins are upregulated and these substrates are found in both the sarcoplasmic and myofibrillar portions of the muscle fiber. Conjugation to ubiquitin has been shown to be the dominant modification of Gly-Gly sites[57]; however, it is possible that some of these sites may have been modified by ISG15 or NEDD8. While the majority of modified lysine residues identified in this study were only found in those TA muscles that overexpressed MuRF1, additional studies are needed to determine whether these changes are the direct result of MuRF1 activity. Our analysis of the MuRF1 ubiquitylome was carried out after 14 days of OE, but we show that MuRF1 expression is significantly higher after only 7 days of OE and loss of CSA is beginning to occur; thus, it is possible that additional E3s were activated and contributed to the ubiquitination of the proteins we identify as putative MuRF1 substrates. The fact that MuRF2, MuRF3, and TRIM25 were found to be modified with *MuRF1* OE suggests that MuRF1 may indirectly impact ubiquitination through the regulation of other E3 ubiquitin ligases. Furthermore, TRIM25 can add ISG15 to target proteins, and trypsin digestion of ISGylated proteins results in a diglycine remnant similar to what occurs with the digestion of ubiquitinated proteins. Thus, it is also possible that some of the MuRF1 substrates we identified were ISGylated and not ubiquitinated. Future studies will focus on confirming that our putative MuRF1 substrates are direct targets of MuRF1 and whether changes in ISGylation occur with *MuRF1* OE.
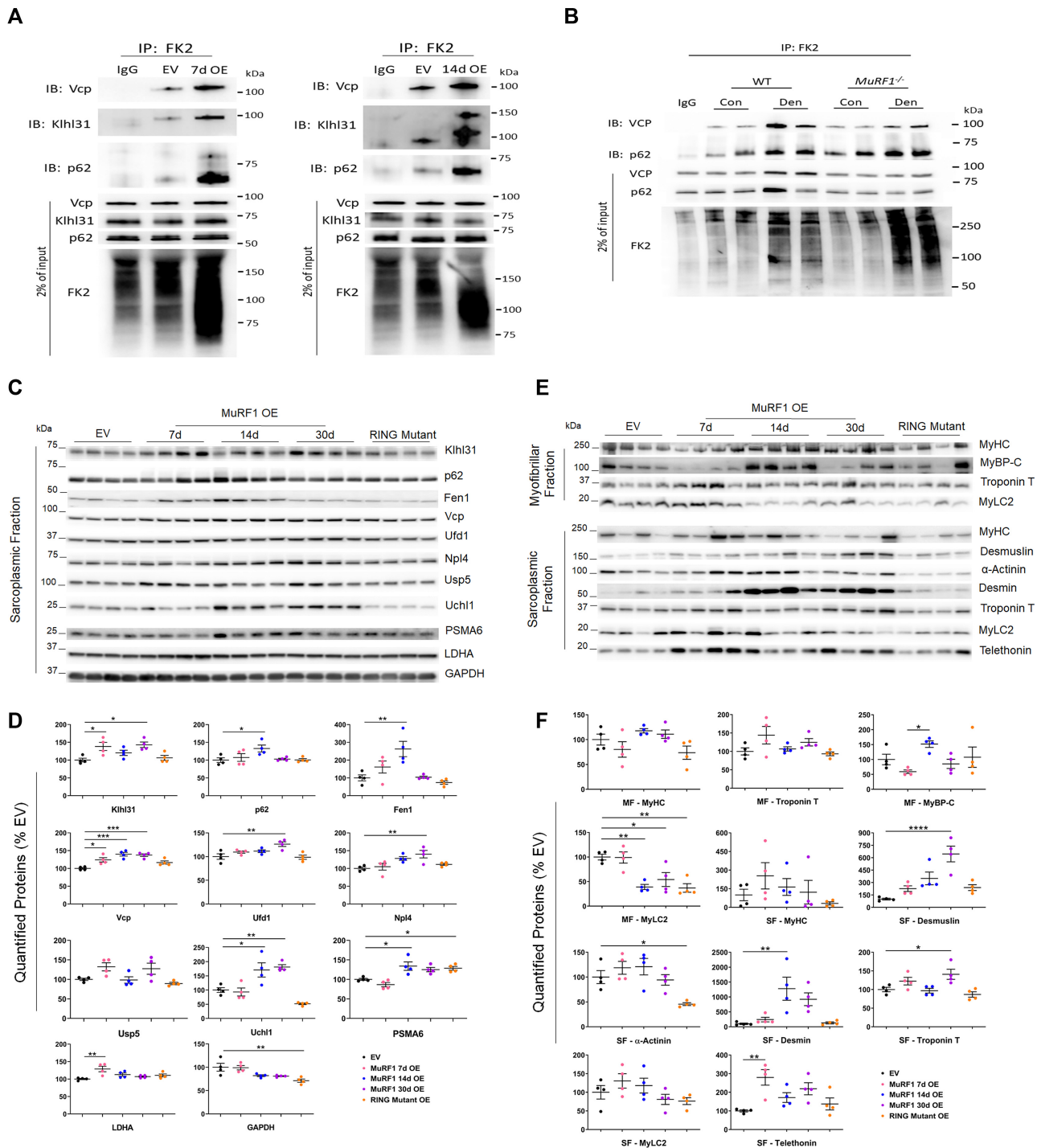
Figure 5. The Majority of MuRF1 Substrates Are Not Degraded, But Ubiquitination Increases the Solubility of Myofilament Proteins. **(A)** Western blots of VCP, Klhl31, and p62 following immunoprecipitation of ubiquitinated proteins from tibialis anterior (TA) muscles electroporated with an empty vector (EV) control plasmid or untagged MuRF1 plasmid for 7 and 14 days; $n = 1$/time point. Increased ubiquitination validates these proteins identified by ubiquitin proteomics as MuRF1 substrates. IgG was used as a control in the immunoprecipitation experiments. IP, immunoprecipitation; IB, immunoblot. **(B)** Western blots of VCP and p62 following immunoprecipitation of ubiquitinated proteins from TA muscles taken from control and 7 day denervated wild-type and $MuRF1^{-/-}$ mice. IgG was used as a control in the immunoprecipitation experiments. WT, wild type. **(C)** Western blots and **(D)** quantification of MuRF1 substrates identified through ubiquitin proteomics that are localized in the sarcoplasm of skeletal muscle. Protein levels of these substrates were analyzed from TA muscles electroporated with an EV plasmid, untagged MuRF1 plasmid for 7, 14, and 30 days, or untagged MuRF1 RING mutant plasmid for 14 days; $n = 4$/group. Data are presented as mean ± SEM with individual points included. P-values were calculated using a one-way ANOVA with Tukey's post hoc test, $^{*}P \leq .05$; $^{**}P \leq .01$; $^{***}P \leq .001$. **(E)** Western blots and **(F)** quantification of contractile proteins identified as MuRF1 substrates through ubiquitin proteomics. Protein levels were analyzed from the myofilament and sarcoplasmic fraction of TA muscles electroporated with an EV plasmid, untagged MuRF1 plasmid for 7, 14, and 30 days, or untagged MuRF1 RING mutant plasmid for 14 days; $n = 4$/group. Data are presented as mean ± SEM with individual points included. P-values were calculated using a one-way ANOVA with Tukey's post hoc test, $^{*}P \leq .05$; $^{**}P \leq .01$; $^{****}P \leq .0001$.

Under normal conditions, MuRF1 binds to titin near the M-line region of the sarcomere. This interaction has been shown to require the coiled-coil domain of MuRF1, and has been suggested to regulate thick filament organization.[46,58] While it remains unclear how ubiquitination regulates MuRF1 function, we noted that the majority of ubiquitin sites on MuRF1 identified by proteomics are located within the coiled-coil domain. We hypothesize that modification of this domain could perturb MuRF1's interaction with titin, resulting in the dissociation of MuRF1 away from titin and leading to disruption of the M-line region of the sarcomere. Further destabilization of the central portion of the sarcomere may occur as MuRF1 ubiquitinates proteins located in this region, such as myomesin and titin. Myomesin acts to stabilize thick filaments by cross-linking these proteins within the M band.[59] Although the MuRF1-modified lysines within myomesin-1 and myomesin-2 are not located within the myosin or titin-binding regions, this ubiquitination event could serve as a signal for ubiquitination by other E3 ligases and the subsequent degradation of these proteins. During denervation, both myomesin-1 and -2 are ubiquitinated at numerous lysines located along the length of each protein, supporting the notion that myomesin is targeted by multiple E3 ligases and sequentially ubiquitinated during muscle atrophy.[54]

Titin is a giant protein that spans half the length of the sarcomere. We found that 63 lysines on titin had increased ubiquitination in response to *MuRF1* OE, with the majority located in the A-band region. While MuRF1 does not appear to target titin for degradation, ubiquitination could disrupt titin's ability to interact with MyBP-C and MyHC, leading to further disorganization of thick filaments and potentially exposing additional ubiquitination sites on these or nearby proteins. Previous studies have determined MyBP-C to be a substrate of MuRF1.[17] Although our proteomics results did not find any ubiquitination sites on MyBP-C, we did observe that MyBP-C protein levels were lower after 7 days of *MuRF1* OE compared with 14 days. Thus, we cannot rule out the possibility that MyBP-C was ubiquitinated by MuRF1 at an earlier time point or that MuRF1 indirectly leads to the degradation of this protein. We found MuRF1 to ubiquitinate MyHC, but this was not accompanied by a decrease in MyHC protein content. The number of ubiquitination sites was low, with 2 sites found on MyHC IIa (myh2), 1 found on MyHC IIx (myh1), and 3 on MyHC IIb (myh4), and all but 1 of these sites are located in the tail region, suggesting that ubiquitination may interrupt its interaction with titin, rather than resulting in degradation. With denervation, muscle atrophy occurs before decreases in MyHC protein are observed,[17] suggesting that thick filament regulatory proteins must be degraded first. The skeletal muscle isoform of myosin regulatory light chain 2 (MyLC2) was found to be ubiquitinated and degraded by MuRF1 and we found this protein to be decreased after 14 days of *MuRF1* OE. The regulatory light chains (RLCs) are located in the neck region of myosin and interact with MyBP-C. Binding of calcium and phosphorylation of the RLCs modulate muscle contraction. The ubiquitination of MyLC2 by MuRF1 occurs in the calcium-binding EF-hand 2 domain. Loss of MyLC2 could have a negative effect on MyBP-C protein levels.

Three additional contractile proteins were found to be ubiquitinated by MuRF1: troponin T and tropomyosin, which are both thin filaments, and desmin, an intermediate filament located primarily at the Z-line. Troponin T binds the troponin complex to tropomyosin, and interestingly, the ubiquitination site on troponin T is located within one of its tropomyosin-binding sites.[60] Although it has been previously shown that degradation of thin filament proteins does not require MuRF1,[17] this ubiquitination

event could lead to thin filament disorganization and ubiquitination on additional sites that promote degradation. Desmin is important for proper alignment of myofibrils and links the myofibrillar proteins to other structures within the muscle fiber, such as mitochondria, nuclei, and the sarcolemma.[59,61] Desmin forms homopolymers or heteropolymers with other intermediate filaments, such as vimentin and nestin.[59] Disassembly of desmin is initiated upon phosphorylation by kinases such as GSK3-β, which leads to ubiquitination by Trim32.[56,62] Phosphorylated and ubiquitinated desmin filaments are then cleaved by calpain-1,[62] resulting in desmin depolymerization and degradation. Our finding that MuRF1 also ubiquitinates desmin indicates that MuRF1 and Trim32 may work together to facilitate the breakdown of desmin and increase sarcomere instability.

In addition to its ubiquitination of sarcomeric proteins, we found MuRF1 to modify a number of metabolic and UPS-related proteins. Studies in both skeletal and cardiac muscle have implicated MuRF1 as a regulator of metabolism,[40,41,45,52] and our finding that MuRF1 ubiquitinates 4 glycolytic enzymes provides further support for MuRF1 regulation of skeletal muscle carbohydrate metabolism. The UPS related proteins discovered to be MuRF1 substrates include the known E3 ubiquitin ligases MuRF2, MuRF3, and TRIM25; proteins that bind to ubiquitinated proteins, such as the deubiquitinases USP5, USP13, and Uchl1; and the adaptor proteins Klhl31 and Klhl41, along with VCP and p62. MuRF1, along with other E3 ligases, is known to ubiquitinate deubiquitinases, but it is unclear whether this modification alters their activity or ability to recognize substrates.[63,64] Polyubiquitination of Klhl41 has been reported and this was found to stabilize nebulin within the sarcomere.[65] Future studies are needed to determine whether MuRF1 is monoubiquitinating or polyubiquitinating its substrates. Klhl31 protein levels were increased at 7 and 30 days of *MuRF1* OE, suggesting that ubiquitination of this protein may protect it from degradation. Numerous lysines on p62 and VCP are also known to be ubiquitinated.[48,57] Lysine 437 on p62 is located at the C-terminal end of its ubiquitin-associated domain, and removal of amino acids 435–438 disables dimerization of p62 and promotes ubiquitin binding.[66] In a similar manner, ubiquitination of K437 by MuRF1 may shift the p62 equilibrium toward its monomeric form and increase its ability to bind ubiquitinated proteins and transport them either to the proteasome or lysosome for degradation. For p62, the two MuRF1 ubiquitination sites found in our study (K13, K437) are the same sites that were found to be ubiquitinated during denervation,[54] suggesting that MuRF1 is responsible for ubiquitination of these residues during atrophy. However, our data also show that p62 ubiquitination increases with denervation even in the absence of MuRF1. More studies are needed to determine whether other E3 ligases can ubiquitinate these same lysine residues or whether the lack of MuRF1 is causing p62 to be ubiquitinated at alternate lysines and how this affects p62 function during muscle atrophy. The fact that p62 was identified as a substrate of MuRF1 is also interesting given that MuRF1 and p62 have been associated with increased endocytosis of acetylcholine receptor subunits.[10,36] Our gene expression data showed that expression of genes associated with the NMJ was upregulated at 14 days of *MuRF1* OE, suggesting that *MuRF1* OE could have affected AChR subunit turnover, which may have contributed to the fiber atrophy. Further studies are needed to determine the link between *MuRF1* OE, p62 ubiquitination, and AChR turnover.

How ubiquitination alters VCP function is unclear. It is thought that ubiquitination could serve as a localization signal or alter its ability to interact with substrates and cofactors.[48] VCP

is known to bind to ubiquitinated proteins, either by itself, or through adaptor proteins such as Ufd1 and Npl4. Often, binding to these ubiquitinated proteins results in their removal from larger complexes/membranes or leads to the unfolding of the ubiquitinated protein for proteasomal degradation.[67] In skeletal muscle, VCP was shown to be involved in the removal of ubiquitinated proteins from the sarcomere, and loss of VCP function in the TA muscle was shown to protect against denervation and starvation-induced atrophy.[50] We hypothesize that ubiquitination of VCP and its cofactors Ufd1 and Npl4 by MuRF1 acts to localize this complex to the sarcomere and aids in its ability to recognize and extract ubiquitinated myofibrillar proteins. Interestingly, we observed ubiquitination of VCP to be decreased in response to denervation in the *MuRF1*$^{-/-}$ mice. Given that muscle loss is attenuated in the *MuRF1*$^{-/-}$ mice with denervation, we envision that MuRF1 and VCP work together to disassemble the sarcomere during muscle atrophy. Future experiments will determine how MuRF1 regulates VCP function.

Although MuRF1 and MAFbx are often discussed together as muscle-specific E3 ligases that are upregulated under atrophy conditions, our data suggest that OE of *MAFbx* alone in vivo is not sufficient to induce muscle atrophy. MAFbx is a member of the Skp1-cullin1-F-box (SCF) family of E3 ubiquitin ligases and, as an F-box protein, is important for substrate recognition.[12,68] F-box proteins often bind to their substrates through specific amino acids sequences that have undergone a post-translational modification (PTM) such as phosphorylation.[69] For ubiquitination to occur, MAFbx forms a complex with Skp1, cullin1, and the E2 enzyme recruiting protein RBX1. While we only overexpressed MAFbx, our findings are consistent with results published in Sartori et al.,[70] who found that transfection of TA with MAFbx alone or together with proteins that form the SCF complex (Skip1, Cul1, and Roc1) did not induce muscle atrophy. In this same study,[70] it was also shown that cotransfection of the TA with MUSA1 (Fbxo30) and SCF complex proteins was insufficient to induce muscle atrophy. It is possible that overexpression of muscle with MAFbx or other F-box E3 ligases in unchallenged muscle does not induce a phenotype because the substrates have not undergone PTM, and are thus not recognized as substrates for ubiquitination. However, recently we showed that transfection of unchallenged TA muscle with Fbxl22, an F-box E3 ligase, resulted in muscle fiber degeneration demonstrating that certain F-box proteins can induce a phenotype when transfected into muscle.[22] Clearly, MAFbx plays an important role in skeletal muscle atrophy, which is distinct from MuRF1. Additional studies are needed to identify the in vivo substrates of MAFbx and to find how ubiquitination of those substrates alters the function and/or structure of skeletal muscle.

Conclusions

In this study, we demonstrate that *MuRF1* overexpression is sufficient to cause muscle atrophy. Using label-free quantitative proteomics, we have generated a comprehensive list of substrates, along with the specific lysines modified by overexpression of MuRF1 in vivo. Our data suggest that MuRF1 ubiquitination alone may not always produce a ubiquitination signature that triggers degradation. However, ubiquitination of a substrate by MuRF1 could: (1) disrupt the organization of the sarcomere, exposing ubiquitination sites on contractile proteins that are normally inaccessible; (2) promote recognition and further ubiquitination of its substrates by other E3 ligases; and/or (3) regulate the activity of other proteolytic pathways, ultimately

leading to an increase in protein degradation and muscle atrophy. These findings provide new insights into the mechanisms by which MuRF1 induces skeletal muscle atrophy. Future experiments will validate whether each substrate identified in this study is a direct target of MuRF1 and will determine the types of ubiquitin chains added by MuRF1. These findings have important implications in the development of therapeutic strategies and provide new avenues for investigations into understanding the molecular mechanisms of muscle atrophy.

Supplementary Material

Supplementary material is available at the *APS Function* online.

Conflict of Interest Statement

S.C.B. is on the scientific advisory board of Emmyon Inc. and a paid consultant of Calico Life Sciences.

Data Availability

The mass spectrometry proteomics data have been deposited to the ProteomeXchange Consortium via the PRIDE partner repository with the dataset identifier: PXD023872. The data underlying this article will be shared on reasonable request to the corresponding author.

References

1. Taillandier D, Combaret L, Pouch MN, Samuels SE, Bechet D, Attaix D. The role of ubiquitin-proteasome-dependent proteolysis in the remodelling of skeletal muscle. *Proc Nutr Soc* 2004;**63**(2):357–361.

2. Budhidarmo R, Nakatani Y, Day CL. RINGs hold the key to ubiquitin transfer. *Trends Biochem Sci* 2012;**37**(2):58–65.

3. Kitajima Y, Tashiro Y, Suzuki N, et al. Proteasome dysfunction induces muscle growth defects and protein aggregation. *J Cell Sci* 2014;**127**(24):5204–5217.

4. Baehr LM, Tunzi M, Bodine SC. Muscle hypertrophy is associated with increases in proteasome activity that is independent of MuRF1 and MAFbx expression. *Front Physiol* 2014;**5**:69.

5. Nury D, Doucet C, Coux O. Roles and potential therapeutic targets of the ubiquitin proteasome system in muscle wasting. *BMC Biochem* 2007;**8**(Suppl 1):S7.

6. Bilodeau PA, Coyne ES, Wing SS. The ubiquitin proteasome system in atrophying skeletal muscle: roles and regulation. *Am J Physiol Cell Physiol* 2016;**311**(3):C392–C403.

7. Centner T, Yano J, Kimura E, et al. Identification of muscle specific ring finger proteins as potential regulators of the titin kinase domain. *J Mol Biol* 2001;**306**(4):717–726.

8. Franke B, Gasch A, Rodriguez D, et al. Molecular basis for the fold organization and sarcomeric targeting of the muscle atrogin MuRF1. *Open Biol* 2014;**4**(3):130172.

9. Mrosek M, Meier S, Ucurum-Fotiadis Z, et al. Structural analysis of B-Box 2 from MuRF1: identification of a novel self-association pattern in a RING-like fold. *Biochemistry* 2008;**47**(40):10722–10730.

10. Khan MM, Strack S, Wild F, et al. Role of autophagy, SQSTM1, SH3GLB1, and TRIM63 in the turnover of nicotinic acetylcholine receptors. *Autophagy* 2014;**10**(1):123–136.

11. Heras G, Namuduri AV, Traini L, et al. Muscle RING-finger protein-1 (MuRF1) functions and cellular localization are regulated by SUMO1 post-translational modification. *J Mol Cell Biol* 2019;**11**(5):356–370.

12. Bodine SC, Latres E, Baumhueter S, et al. Identification of ubiquitin ligases required for skeletal muscle atrophy. *Science* 2001;**294**(5547):1704–1708.

13. Baehr LM, Furlow JD, Bodine SC. Muscle sparing in muscle RING finger 1 null mice: response to synthetic glucocorticoids. *J Physiol* 2011;**589**(19):4759–4776.

14. Sacheck JM, Hyatt J-PK, Raffaello A, et al. Rapid disuse and denervation atrophy involve transcriptional changes similar to those of muscle wasting during systemic diseases. *FASEB J* 2007;**21**(1):140–155.

15. Lecker SH, Jagoe RT, Gilbert A, et al. Multiple types of skeletal muscle atrophy involve a common program of changes in gene expression. *FASEB J* 2004;**18**(1):39–51.

16. Hwee DT, Gomes AV, Bodine SC. Cardiac proteasome activity in muscle ring finger-1 null mice at rest and following synthetic glucocorticoid treatment. *Am J Physiol Endocrinol Metab* 2011;**301**(5):E967–E977.

17. Cohen S, Brault JJ, Gygi SP, et al. During muscle atrophy, thick, but not thin, filament components are degraded by MuRF1-dependent ubiquitylation. *J Cell Biol* 2009;**185**(6):1083–1095.

18. Iconomou M, Saunders DN. Systematic approaches to identify E3 ligase substrates. *Biochem J* 2016;**473**(22):4083–4101.

19. Vere G, Kealy R, Kessler BM, Pinto-Fernandez A. Ubiquitomics: an overview and future. *Biomolecules* 2020;**10**(10):1453.

20. Ebert SM, Monteys AM, Fox DK, et al. The transcription factor ATF4 promotes skeletal myofiber atrophy during fasting. *Mol Endocrinol* 2010;**24**(4):790–799.

21. Seaborne RA, Hughes DC, Turner DC, et al. UBR5 is a novel E3 ubiquitin ligase involved in skeletal muscle hypertrophy and recovery from atrophy. *J Physiol* 2019;**597**(14):3727–3749.

22. Hughes DC, Baehr LM, Driscoll JR, Lynch SA, Waddell DS, Bodine SC. Identification and characterization of Fbxl22, a novel skeletal muscle atrophy-promoting E3 ubiquitin ligase. *Am J Physiol Cell Physiol* 2020;**319**(4):C700–C719.

23. Gomes AV, Waddell DS, Siu R, et al. Upregulation of proteasome activity in muscle RING finger 1-null mice following denervation. *FASEB J* 2012;**26**(7):2986–2999.

24. Wen Y, Murach KA, IJV Jr., et al. MyoVision: software for automated high-content analysis of skeletal muscle immunohistochemistry. *J Appl Physiol* 2018;**124**(1):40–51.

25. Baehr LM, West DW, Marcotte G, et al. Age-related deficits in skeletal muscle recovery following disuse are associated with neuromuscular junction instability and ER stress, not impaired protein synthesis. *Aging* 2016;**8**(1):127–146.

26. Baehr LM, West DWD, Marshall AG, Marcotte GR, Baar K, Bodine SC. Muscle-specific and age-related changes in protein synthesis and protein degradation in response to hindlimb unloading in rats. *J Appl Physiol* 2017;**122**(5):1336–1350.

27. Hughes DC, Marcotte GR, Baehr LM, et al. Alterations in the muscle force transfer apparatus in aged rats during unloading and reloading: impact of microRNA-31. *J Physiol* 2018;**596**(14):2883–2900.

28. Roberts MD, Young KC, Fox CD, et al. An optimized procedure for isolation of rodent and human skeletal muscle sarcoplasmic and myofibrillar proteins. *J Biol Methods* 2020;**7**(1):e127.

29. Maia TM, Staes A, Plasman K, et al. Simple peptide quantification approach for MS-based proteomics quality control. *ACS Omega* 2020;**5**(12):6754–6762.

30. Chiva C, Olivella R, Borràs E, et al. QCloud: a cloud-based quality control system for mass spectrometry-based proteomics laboratories. *PLoS One* 2018;**13**(1):e0189209.

31. Cox J, Hein MY, Luber CA, Paron I, Nagaraj N, Mann M. Accurate proteome-wide label-free quantification by delayed normalization and maximal peptide ratio extraction, termed MaxLFQ. *Mol Cell Proteomics* 2014;**13**(9):2513–2526.

32. Tusher VG, Tibshirani R, Chu G. Significance analysis of microarrays applied to the ionizing radiation response. *Proc Natl Acad Sci USA* 2001;**98**(9):5116–5121.

33. Huang da W, Sherman BT, Lempicki RA. Systematic and integrative analysis of large gene lists using DAVID bioinformatics resources. *Nat Protoc* 2009;**4**(1):44–57.

34. Huang da W, Sherman BT, Lempicki RA. Bioinformatics enrichment tools: paths toward the comprehensive functional analysis of large gene lists. *Nucleic Acids Res* 2009;**37**(1):1–13.

35. Deshaies RJ, Joazeiro CAP. RING domain E3 ubiquitin ligases. *Annu Rev Biochem* 2009;**78**(1):399–434.

36. Rudolf R, Bogomolovas J, Strack S, et al. Regulation of nicotinic acetylcholine receptor turnover by MuRF1 connects muscle activity to endo/lysosomal and atrophy pathways. *AGE* 2013;**35**(5):1663–1674.

37. Moresi V, Williams AH, Meadows E, et al. Myogenin and class II HDACs control neurogenic muscle atrophy by inducing E3 ubiquitin ligases. *Cell* 2010;**143**(1):35–45.

38. Bongers KS, Fox DK, Ebert SM, et al. Skeletal muscle denervation causes skeletal muscle atrophy through a pathway that involves both Gadd45a and HDAC4. *Am J Physiol Endocrinol Metab* 2013;**305**(7):E907–E915.

39. Bullard SA, Seo S, Schilling B, et al. Gadd45a protein promotes skeletal muscle atrophy by forming a complex with the protein kinase MEKK4. *J Biol Chem* 2016;**291**(34):17496–17509.

40. Hirner S, Krohne C, Schuster A, et al. MuRF1-dependent regulation of systemic carbohydrate metabolism as revealed from transgenic mouse studies. *J Mol Biol* 2008;**379**(4):666–677.

41. Koyama S, Hata S, Witt CC, et al. Muscle RING-finger protein-1 (MuRF1) as a connector of muscle energy metabolism and protein synthesis. *J Mol Biol* 2008;**376**(5):1224–1236.

42. Witt SH, Granzier H, Witt CC, Labeit S. MURF-1 and MURF-2 target a specific subset of myofibrillar proteins redundantly: towards understanding MURF-dependent muscle ubiquitination. *J Mol Biol* 2005;**350**(4):713–722.

43. Kedar V, McDonough H, Arya R, Li HH, Rockman HA, Patterson C. Muscle-specific RING finger 1 is a bona fide ubiquitin ligase that degrades cardiac troponin I. *Proc Natl Acad Sci USA* 2004;**101**(52):18135–18140.

44. Rubel CE, Schisler JC, Hamlett ED, et al. Diggin' on u(biquitin): a novel method for the identification of physiological E3 ubiquitin ligase substrates. *Cell Biochem Biophys* 2013;**67**(1):127–138.

45. Rodríguez JE, Liao J-Y, He J, et al. The ubiquitin ligase MuRF1 regulates PPARα activity in the heart by enhancing nuclear export via monoubiquitination. *Mol Cell Endocrinol* 2015;**413**:36–48.

46. Mrosek M, Labeit D, Witt S, et al. Molecular determinants for the recruitment of the ubiquitin-ligase MuRF-1 onto M-line titin. *FASEB J* 2007;**21**(7):1383–1392.

47. Stevens M, Franke B, Skorupka KA, et al. Exploration of the TRIM fold of MuRF1 using EPR reveals a canonical antiparallel structure and extended COS-box. *J Mol Biol* 2019;**431**(15):2900–2909.

48. Hanzelmann P, Schindelin H. The interplay of cofactor interactions and post-translational modifications in the regulation of the AAA+ ATPase p97. *Front Mol Biosci* 2017;**4**:21.

49. Meyer H, Weihl CC. The VCP/p97 system at a glance: connecting cellular function to disease pathogenesis. *J Cell Sci* 2014;**127**(Pt 18):3877–3883.

50. Piccirillo R, Goldberg AL. The p97/VCP ATPase is critical in muscle atrophy and the accelerated degradation of muscle proteins. *EMBO J* 2012;**31**(15):3334–3350.

51. Liu WJ, Ye L, Huang WF, et al. p62 links the autophagy pathway and the ubiquitin–proteasome system upon ubiquitinated protein degradation. *Cell Mol Biol Lett* 2016;**21**(1):29.

52. Witt CC, Witt SH, Lerche S, Labeit D, Back W, Labeit S. Cooperative control of striated muscle mass and metabolism by MuRF1 and MuRF2. *EMBO J* 2008;**27**(2):350–360.

53. Nowak M, Suenkel B, Porras P, et al. DCAF8, a novel MuRF1 interaction partner, promotes muscle atrophy. *J Cell Sci* 2019;**132**(17):jcs233395.

54. Lang F, Aravamudhan S, Nolte H, et al. Dynamic changes in the mouse skeletal muscle proteome during denervation-induced atrophy. *Dis Model Mech* 2017;**10**(7):881–896.

55. Polge C, Cabantous S, Deval C, et al. A muscle-specific MuRF1-E2 network requires stabilization of MuRF1-E2 complexes by telethonin, a newly identified substrate. *J Cachexia Sarcopenia Muscle* 2018;**9**(1):129–145.

56. Cohen S, Zhai B, Gygi SP, Goldberg AL. Ubiquitylation by Trim32 causes coupled loss of desmin, Z-bands, and thin filaments in muscle atrophy. *J Cell Biol* 2012;**198**(4):575–589.

57. Kim W, Bennett Eric J, Huttlin Edward L, et al. Systematic and quantitative assessment of the ubiquitin-modified proteome. *Mol Cell* 2011;**44**(2):325–340.

58. McElhinny AS, Kakinuma K, Sorimachi H, Labeit S, Gregorio CC. Muscle-specific RING finger-1 interacts with titin to regulate sarcomeric M-line and thick filament structure and may have nuclear functions via its interaction with glucocorticoid modulatory element binding protein-1. *J Cell Biol* 2002;**157**(1):125–136.

59. Henderson CA, Gomez CG, Novak SM, Mi-Mi L, Gregorio CC. Overview of the muscle cytoskeleton. *Compr Physiol* 2017;**7**(3):891–944.

60. Jin JP, Chong SM. Localization of the two tropomyosin-binding sites of troponin T. *Arch Biochem Biophys* 2010;**500**(2):144–150.

61. Hughes DC, Wallace MA, Baar K. Effects of aging, exercise, and disease on force transfer in skeletal muscle. *Am J Physiol Endocrinol Metab* 2015;**309**(1):E1–E10.

62. Aweida D, Rudesky I, Volodin A, Shimko E, Cohen S. GSK3-β promotes calpain-1–mediated desmin filament depolymerization and myofibril loss in atrophy. *J Cell Biol* 2018;**217**(10):3698–3714.

63. Loch CM, Strickler JE. A microarray of ubiquitylated proteins for profiling deubiquitylase activity reveals the critical roles of both chain and substrate. *Biochim Biophys Acta* 2012;**1823**(11):2069–2078.

64. Haq S, Ramakrishna S. Deubiquitylation of deubiquitylases. *Open Biol* 2017;**7**(6):170016.

65. Ramirez-Martinez A, Cenik BK, Bezprozvannaya S, et al. KLHL41 stabilizes skeletal muscle sarcomeres by nonproteolytic ubiquitination. *eLife* 2017;**6**:e26439.

66. Isogai S, Morimoto D, Arita K, et al. Crystal structure of the ubiquitin-associated (UBA) domain of p62 and its interaction with ubiquitin. *J Biol Chem* 2011;**286**(36):31864–31874.

67. van den Boom J, Meyer H. VCP/p97-mediated unfolding as a principle in protein homeostasis and signaling. *Mol Cell* 2018;**69**(2):182–194.

68. Gomes MD, Lecker SH, Jagoe RT, Navon A, Goldberg AL. Atrogin-1, a muscle-specific F-box protein highly expressed during muscle atrophy. *Proc Natl Acad Sci USA* 2001;**98**(25):14440–14445.

69. Nguyen KM, Busino L. The biology of F-box proteins: the SCF family of E3 ubiquitin ligases. *Adv Exp Med Biol* 2020;**1217**:111–122.

70. Sartori R, Schirwis E, Blaauw B, et al. BMP signaling controls muscle mass. *Nat Genet* 2013;**45**(11):1309–1318.